High-resolution spectroscopic study of the C 0# and D 1 Rydberg states of KrXe and of the X 1/2 and A1 3/2 states of KrXe#

Author(s):
Piticco, Lorena; Merkt, Frédéric

Publication date:
2013-02

Permanent link:
https://doi.org/10.3929/ethz-a-010780475

Originally published in:
Journal of Molecular Spectroscopy 284-285, https://doi.org/10.1016/j.jms.2012.12.003

Funding acknowledgement:
135342 - Rydberg states, VUV laser spectroscopy and photoionization dynamics (SNF)

The following article appeared in *J. Mol. Spectrosc.* **284-285**, 37-53 (2013) and may be found at http://dx.doi.org/10.1016/j.jms.2012.12.003.

High resolution spectroscopic study of the C 0^+ and D 1 Rydberg states of KrXe and of the X 1/2 and A_1 3/2 states of $KrXe^+$

Lorena Piticco and Frédéric Merkt

Laboratorium für Physikalische Chemie, ETH Zürich, 8093 Zürich

Abstract

The electronic spectrum of the C 0^+, D $1 \leftarrow$ X 0^+ transitions of KrXe has been studied at high resolution in the vicinity of the Kr($^1S_0$) + Xe 6p[5/2]$_2$ dissociation limit by resonance-enhanced (1+1′) two-photon ionization spectroscopy. The rotational structure of 13 bands, 5 and 8 of which correspond to transitions to levels of 0^+ and 1 symmetry, respectively, were observed in the spectra of several isotopomers, and the hyperfine structure in the spectrum of the $\Omega = 1$ levels of $^{84}Kr^{129}Xe$ was determined. The five transitions to levels of 0^+ symmetry form a regular progression of bands characterized by a regular rotational structure and corresponding to high vibrational levels (with $v = 16 - 20$) of the C 0^+ state. The C 0^+ state is found to possess significant X 1/2, A_1 3/2 and A_2 1/2 ion-core character in combination with an excited electron of 6pσ, 6pπ and 6sσ character, respectively, and to correlate adiabatically to the Kr($^1S_0$) + Xe 6s[1/2]$_1^o$ dissociation limit. The transition to the eight levels of $\Omega = 1$ symmetry form a very irregular progression both as far as spectral positions and intensities are concerned. Rotational levels of f-symmetry, accessed via Q-branch transitions, are weakly predissociated by a repulsive level associated with the Kr($^1S_0$) + Xe 6s[1/2]$_0^o$ limit. A local perturbation in the rotational structure of the fourth level of $\Omega = 1$ symmetry enabled the identification of a so far unobserved predissociative level of $\Omega = 1$ or $\Omega = 2$ symmetry with band center near 77318.5 cm^{-1}. The determination of the band centers, rotational constants and isotopic shifts of the $\Omega = 1$ levels led to the conclusion that the level structure is affected by homogeneous perturbations and that at least two electronic states of $\Omega = 1$ symmetry contribute to the spectrum of KrXe in this spectral region. Modelling the observed rovibronic structure using a coupling model involving low vibrational levels of a weakly bound $\Omega = 1$ state associated with the Kr($^1S_0$) + Xe 6s[1/2]$_1^o$ dissociation limit and high vibrational levels of a more strongly bound state associated with the Kr($^1S_0$) + Xe 6p[5/2]$_2$ dissociation limit enabled us to reproduce the observed values of the rotational constants, vibronic positions and intensity distribution in a qualitatively satisfactory manner. However, the model failed to account for the observed isotopic shifts. Rotationally resolved photoelectron spectra of the $KrXe^+$ X 1/2 $\leftarrow$ KrXe C 0^+ and $KrXe^+$ A_1 3/2 $\leftarrow$ KrXe C 0^+ ionizing transitions were recorded from selected rotational levels of selected isotopomers of KrXe. The rotational levels of the X 1/2 state of $KrXe^+$ group as pairs of levels of opposite parity and have a spin-rotation coupling constant γ of approximately $-2B$, as a consequence of pure precession. The rotational level structure of the low-lying electronic states of $KrXe^+$ thus appear to form the same patterns as the corresponding states of $ArXe^+$.

Keywords: rare-gas dimer ions, PFI-ZEKE photoelectron spectroscopy, rotational structure, predissociation

1. Introduction

This article is devoted to a study of the electronic spectrum of KrXe in the vicinity of the Xe $6s'[1/2]^o_1$ + Kr($^1S_0$) dissociation limit and to its comparison with the spectrum of ArXe in the same region. The main scientific goal of this investigation is to characterize excited electronic states of diatomic molecules that can be regarded, in first approximation, as consisting of an electronically excited atom weakly interacting with a ground-state atom with a closed-shell electronic configuration. The electronically excited states of the heteronuclear rare-gas dimers located close to one of the dissociation limits Rg′* + Rg($^1S_0$) (Rg, Rg′ = Ne, Ar, Kr, Xe and Rn), and in particular the C and D states of ArXe and KrXe, are ideal systems for such an investigation.

This scientific goal has been pursued in several previous investigations of the low-lying electronic states of KrXe, most notably in studies by VUV absorption and emission spectroscopy [1, 2, 3, 4], resonant multiphoton ionization spectroscopy [5, 6, 7, 8, 9, 10, 11, 12, 13, 14, 15] and photoelectron spectroscopy [16, 17]. In these studies, the vibrational structure of the electronic spectra could be resolved, insight could be gained into the main properties of the electronically excited states, and the dominant spectral perturbations could be identified. To illustrate the type of information that could be obtained in these investigations, Figure 1 compares the (1+1′) resonant two-photon ionization spectra of the C, D ← X band systems of $^{40}Ar^{129}Xe$ (from Ref. [18]) and $^{84}Kr^{132}Xe$ (from Ref. [9]) in the vicinity of the Xe $6s'[1/2]^o_1$ + Rg($^1S_0$) dissociation limit in the region 77000-77300 cm^{-1}.

These spectra both consist of two vibrational progressions associated with the C 1 ← X and D 0^+ ← X transitions in ArXe and the C 0^+ ← X and D 1 ← X transitions in the case of KrXe. In these spectra, the progressions attributed to the 0^+ state appear regular and those attributed to the $\Omega = 1$ states appear strongly perturbed. If the assignment derived in previous studies [14, 8] are correct, the ordering of the $\Omega = 0^+$ and $\Omega = 1$ states reverses in going from ArXe to KrXe, and the 0^+ state is much more strongly bound in KrXe than in ArXe, whereas the opposite is true for the $\Omega = 1$ state. The spectrum of KrXe in Figure 1b has several unassigned lines, marked with asterisks, in the region of the D 1 ← X 0^+ transition.

An experiment in which the rotational structure can be resolved in addition to the vibrational structure brings several advantages in the study of perturbed spectra that were already exploited in our studies of ArXe presented in Refs. [19] and [20]: Resolving the rotational structure enables the unambiguous assignment of the electronic symmetry, the identification of perturbations, the determination of internuclear distances and the possibility to record rotationally resolved photoelectron spectra. The general considerations drawn from the previous studies of the electronic spectrum of ArXe and KrXe and from the theoretical studies described in Refs. [21, 22, 23] are that the electronic spectrum of the heteronuclear rare-gas dimers is too complex to be described by solely considering the interaction between an excited and a ground state atom using long-range electrostatic interaction series. Instead, electronically excited states of the rare-gas dimers are more conveniently and realistically described as interacting molecular Rydberg states in which an electron in a large, diffuse orbital weakly interacts with a strongly bound rare-gas dimer

molecular cation. An example is the C 1 state of ArXe, the potential-energy function of which can be approximately described in the region between 3.5 and 4.5 Å as resulting from an interaction between the dominant [A_1 3/2]6pσ and [A_2 1/2]6sσ configurations (see Ref. [19]).

The work presented in this article had two specific goals: First, to obtain rotationally resolved electronic spectra of KrXe in the region of the C 0^+ and D 1 states depicted in Figure 1b and use the information contained in the rotational structure to extract the structural and interaction parameters needed to describe the behavior of these states. Second, to study the spin-rovibronic energy level structure of $KrXe^+$ and compare the observed spectral patterns with those recently determined in $ArXe^+$. The two lowest-lying $\Omega = 1/2$ states of $ArXe^+$ (the X 1/2 and A_2 1/2 states) were indeed found [20] to approximately be described by a limiting case [24, 25] of $^2\Pi - {}^2\Sigma$ interaction for which the spin-rotation coupling constant γ of the X 1/2 state and the Λ (Ω)-doubling constant p of the A_2 1/2 state are both approximately equal to $-2B$. In this pure-precession situation, also observed in $HeAr^+$ [26] and $HeNe^+$ [27], the splittings of the rotational levels of the X and A_2 states become too small to be observed in the PFI-ZEKE photoelectron spectra. $KrXe^+$ represents another molecular system in which this situation may be encountered.

Measurements of the rotational structure in the photoelectron spectrum of molecules with rotational constants smaller than $0.1\,\mathrm{cm}^{-1}$ represents a challenge and requires resonant multiphoton excitation through selected rotational levels of (long-lived) intermediate states to avoid spectral congestion. Our results presented in Section 5 on the $v^+ = 5, 22$ and 28 vibrational levels of the X 1/2 state of $KrXe^+$, which have rotational constants of $\sim 0.03\,\mathrm{cm}^{-1}$ demonstrate that such measurements are possible.

The nomenclature used to label the electronic states of the rare-gas atoms is $np^{(\prime)}[K]^{(\mathrm{o})}_J$, where K is the angular-momentum quantum number resulting from the vector addition $\vec{K} = \vec{J^+} + \vec{l}$ (J^+ is the total angular-momentum quantum number of the ion-core state the Rydberg series converge to, with $J^+ = 3/2$ and 1/2 for the lower $^2P_{3/2}$ and upper $^2P_{1/2}$ spin-orbit components, respectively), the $'$ sign indicates series converging on the $^2P_{1/2}$ spin-orbit component, and the label $^{\mathrm{o}}$ designates states of odd parity.

2. Experiment

To record rotationally resolved spectra of the C $0^+ \leftarrow$ X 0^+ and D 1 $\leftarrow$ X 0^+ transitions of KrXe we used a resonant ($1_{\mathrm{VUV}} + 1'$) two-photon excitation sequence which requires a tunable narrow-bandwidth vacuum-ultraviolet (VUV) laser system for the first excitation step and a fixed-frequency visible or UV laser to ionize the molecules in the second step. The same excitation sequence was employed to record the PFI-ZEKE photoelectron spectra of KrXe but the wave number of the VUV laser was kept fixed at the position of selected rovibronic transitions of selected isotopomers of KrXe and the frequency of the visible or UV laser was scanned across the ionization thresholds. The experimental procedure was the same as used in our study of ArXe [20] and described in detail in Refs. [28, 29].

The VUV radiation was generated by resonance-enhanced sum-frequency mixing ($\tilde{\nu}_{\mathrm{VUV}} = 2\tilde{\nu}_{\mathrm{UV}} + \tilde{\nu}_2$) in Kr. The cw outputs of two commercial single-mode ring dye lasers were pulse-amplified using chains of three dye amplifi-

cation stages pumped by the second harmonic (wavelength λ = 532 nm) of a Nd:YAG laser at a repetition rate of 25 Hz. The four-wave mixing process was resonantly enhanced at the two-photon level by locking the wave number $\tilde{\nu}_{UV} = 3\tilde{\nu}_1$ of the tripled output of the first ring dye laser to the position $2\tilde{\nu}_{UV}$ = 94092.906 cm^{-1}, which corresponds to the $4p^5$ ($^2P_{3/2}$) 5p[1/2]$_0$ ← $4p^6$ $^1S_0$ two-photon resonance of atomic krypton. The pulse-amplified output of the second ring dye laser (wave number $\tilde{\nu}_2$) and the beam of wave number $\tilde{\nu}_1$ were recombined using a dichroic mirror and focused into a cell containing the nonlinear Kr gas at a background pressure of 40 mbar. A LiF lens was placed at the exit of the cell to recollimate the diverging VUV beam. The difference-frequency VUV beam was separated from the fundamental beams and beams generated in other nonlinear optical processes using a LiF prism placed in a monochromator chamber and was directed toward the photoexcitation region where it intersected the probe gas beam at right angles.

The rare-gas dimers were produced in a supersonic expansion of a gas mixture of Kr and Xe (mixing ratio 4:1). The supersonic beam was obtained by expanding the gas mixture from a high-pressure region into vacuum using a pulsed valve and entered the photoexcitation region through a skimmer. The supersonic expansion resulted in a quasithermal population of the rotational levels of the KrXe dimers formed in the beam characterized by a rotational temperature of $T_{rot} \sim 3$ K.

Photoexcitation took place in the middle of a cylindrical electrode stack consisting of five equidistant, resistively coupled stainless-steel extraction plates. The ions produced after photoionization were extracted by applying pulsed voltages of positive polarity on the repeller plate and were detected at the end of a time-of-flight (TOF) tube using a microchannel-plate (MCP) detector. The resolution of the TOF mass spectrometer was sufficient to fully separate the ion signals of KrXe isotopomers differing by 1 mass unit. By setting adequate temporal gates in the TOF spectra and monitoring the corresponding ion signals as a function of the laser wave number, spectra of selected isotopomers could be recorded, as illustrated in Figure 2 which shows spectra of the C 0$^+$ (v' = 18) ← X 0$^+$ transition of KrXe. All spectra displayed in Fig. 2 reveal more than one band, because several isotopomers of KrXe have almost the same mass. For instance, spectra of both ^{86}Kr^{132}Xe and ^{82}Kr^{136}Xe are recorded in the 218 u mass channel.

To record rotationally resolved photoelectron spectra from selected rotational levels of selected isotopomers, we used the technique of PFI-ZEKE photoelectron spectroscopy [30] in combination with multipulse electric-field-ionization sequences designed to achieve a spectral resolution of ~0.1 cm^{-1} [31]. The pulsed electric field sequences and the procedure to correct for the field-induced shifts of the ionization thresholds were the same as those used in our study of the photoelectron spectrum of ArXe and are described in detail in Ref. [20].

3. The C 0$^+$ ← X 0$^+$ band system of KrXe

Each band of the C 0$^+$ ← X 0$^+$ transition visible in the spectrum presented in Figure 1b was recorded at high resolution for several isotopomers. As typical illustrations, rotationally resolved (1+1′) REMPI spectra of the C 0$^+$ (v' = 16) ← X 0$^+$ (v'' = 0) and C 0$^+$ (v' = 20) ← X 0$^+$ (v'' = 0) transitions are displayed as inverted traces in Figure 3

(a) and (b), respectively. These spectra were recorded by monitoring the $KrXe^+$ ion signal in the 216 u mass channel which corresponds primarily to the $^{84}Kr^{132}Xe$ isotopomer (15.33 % relative natural abundance [32]) with a weaker contribution of the $^{82}Kr^{134}Xe$ isotopomer (1.21 % relative natural abundance).

The absence of Q-branch lines and the observation of P(1) lines in these spectra enables one to immediately conclude that the transition is a parallel $0^+ \leftarrow 0^+$ transition which, in turn, proves that the C state has 0^+ electronic symmetry. The P branches are characterized by a pronounced bandhead at low J'' values, which indicates that the rotational constants of the C state in the range $v' = 16 - 20$ are larger than in the X 0^+ ($v'' = 0$) ground state and that the equilibrium internuclear separation of the C state is significantly shorter than that of the X state.

No obvious perturbation of the rovibrational structure of the C 0^+ ($v' = 16 - 20$) levels could be detected, and a standard analysis of the spectral positions using

$$\tilde{\nu} = \tilde{\nu}_{v'v''} + (E'_{\rm rot}(v', J') - E''_{\rm rot}(v'', J''))/hc \tag{1}$$

and

$$\frac{E_{\rm rot}(v, J)}{hc} = B_v J(J+1) - D_v J^2 (J+1)^2 \ , \tag{2}$$

led to the values of the rotational constants B''_0 and B'_v, the centrifugal distortion constants D''_0 and D'_v and the band centers listed in Table 1 for the isotopomers $^{84}Kr^{129}Xe$, $^{84}Kr^{132}Xe$ and $^{84}Kr^{136}Xe$. In the weighted least-squares fits that led to these constants, we included, for the $^{84}Kr^{129}Xe$ and $^{84}Kr^{132}Xe$ isotopomers, the ground-state rotational transition frequencies obtained by Fourier-transform microwave spectroscopy by Jäger *et al.* [33]. Because of the much larger weights given to the microwave transitions, the rotational and centrifugal distortion constants B''_0 and D''_0 obtained in the least-squares fits correspond exactly to those determined in Ref. [33]. Fits including only the VUV spectroscopic data led to a fully consistent set of molecular constants, but the values of B''_0 and D''_0 were not defined as precisely (*i.e.,* with as many significant digits) than fits including both VUV and microwave transition frequencies. The absence of microwave spectroscopic data for the $^{84}Kr^{136}Xe$ isotopomer resulted in larger uncertainties for the ground-state constants of that isotopomer. Figure 3 also shows spectra calculated with the molecular constants listed in Table 1. The line intensities were calculated using the standard expressions for the Hönl-London factors [34, 35] and assuming a Boltzmann distribution of ground state levels at a rotational temperature of 3K. The calculated spectra are in good agreement with the experimental spectra.

The spectrum of the C $0^+ \leftarrow$ X 0^+ transition consists exclusively of transitions to highly excited vibrational levels with $v' > 15$ (see Figure 1b). The vibrational assignments presented in Figure 1b were adopted from earlier work [14, 8]. The isotopic shifts of the band centers listed in Table 1 were found to be consistent with these earlier assignments. One must, however, bear in mind that absolute vibrational assignments based on measurements of isotopic shifts of high vibrational levels can easily lead to errors in the vibrational quantum number by one or two units. Extrapolating the vibrational structure to $v' = 0$ using either one anharmonicity constant ($\omega_e x_e$) or two ($\omega_e x_e$

and $\omega_e y_e$) led to harmonic frequencies of ~95 cm^{-1} and ~120 cm^{-1} with $\omega_e x_e$ values of ~1.75 cm^{-1} and ~3.4 cm^{-1}, respectively, which, in turn, imply dissociation energies of ~1300 cm^{-1} and 1100 cm^{-1}, respectively. The $v' = 20$ level of the C 0^+ state can thus be estimated to lie within ~200 cm^{-1} of the dissociation limit. We therefore conclude that the C 0^+ state must correlate adiabatically to the Kr($^1S_0$) + Xe 6s′[1/2]$^o_1$ dissociation limit.

The dissociation limits of KrXe located in the vicinity of 77000 cm^{-1} are given in Table 2, which also indicates the symmetry of the corresponding molecular states in Hund's case (c) nomenclature. The dissociation energies D_e of the X 1/2, A_1 3/2 and A_2 1/2 states of $KrXe^+$ were determined to be 3220.8 cm^{-1}, 732.2 cm^{-1} and 2018.4 cm^{-1}, respectively [9] with harmonic frequencies ω_e of 115.2 cm^{-1}, 41.0 cm^{-1} and 86.4 cm^{-1}, respectively. Comparison of these values with the values estimated for the C 0^+ state makes it clear that this state cannot be adequately described as a Rydberg state with a potential-energy function corresponding closely to that of one of the ionic states: The estimated dissociation energy is much smaller than expected for a [X 1/2] and [A_1 3/2] ion core. The harmonic frequency, on the other hand, is too large for an [A_2 1/2] ion core. The C 0^+ state must therefore be of mixed [A_2 1/2]6sσ, [A_1 3/2]6pπ and [X 1/2]6pσ Rydberg character (see Table 2) and its potential must result from interactions involving at least two, and probably more than two, Rydberg states. Considering the intensity distribution measured by photoionization and PFI-ZEKE photoelectron spectroscopy in Ref. [9] from the C 0^+ ($v' = 19$) level (see Figures 4 and 6 of Ref. [9]) leads to a similar conclusion, and suggests that the C 0^+ state consists of [X 1/2], [A_2 1/2] and [A_1 3/2] ion-core contributions, at least in the region of internuclear distances corresponding to the $v' = 19$ and 20 levels of the C 0^+ state (*i.e.,* around 4 Å). The existence of several close-lying ion-core states in $KrXe^+$ inevitably leads to low-lying Rydberg states being subject to strong R-dependent configurational mixing. The rotationally resolved PFI-ZEKE photoelectron spectra of the X 1/2 ($v^+ = 5, 22, 28$) ← C 0^+ ($v' = 19$) and A_1 3/2 ($v^+ = 3, 4$) ← C 0^+ ($v' = 19$) transitions presented in Section 5 provide additional information and support these conclusions.

4. The D 1 ← X 0^+ band system of KrXe

The (1+1′) REMPI spectrum of the D 1 ← X 0^+ transition displayed in Figure 1b is characterized by a strongly perturbed intensity distribution and by irregularly spaced vibrational lines. In their analysis of the D 1 ← X 0^+ band system, Tsuchizawa *et al.* [14] assigned the four main transitions to a single vibrational progression and proposed to assign the lowest member of this progression to $v = 0$ without, however, establishing the absolute vibrational numbering with certainty. In the analysis of the same progression, Mao *et al.* [8] proposed to assign the lowest member of this progression to $v' = 1$. From a measurement of this progression, Zehnder *et al.* [9] concluded that the corresponding D 1 vibrational level was unlikely to be $v' = 0$ or $v' = 1$. They labeled the successive members of this progression with vibrational quantum number $v' = m, m+1, m+2$ and $m+3$. In addition to this main progression of four lines, Zehnder *et al.* [9] also observed four very weak lines, marked with asterisks in Figure 1b, but could not assign them and speculated that they might be vibrational levels of a different electronic state or vibrational levels associated with another potential well of either the C or D states. These previous studies indicated that the VUV spectrum

of KrXe in the region 77250-77300 cm^{-1} is very difficult to assign, and the goal of the high-resolution spectroscopic study presented in this section was to obtain information on the rotational structure that may help to (i) unambiguously determine the electronic symmetry of the upper levels of all eight transitions observed in Figure 1b, (ii) find out whether some of the observed bands might be hot bands and to establish, on the basis of the rotational constants, whether they correspond to one, two or even more different vibrational progressions and to identify perturbations, and (iii) obtain precise values of the isotopic shifts and derive absolute vibrational assignments. In the discussion of the eight vibrational bands observed near the D-X transition we refer to the four main bands with the labels m, $m + 1$, $m + 2$ and $m + 3$ and to the four weak bands with *, **, *** and **** in order of increasing energy.

4.1. Rotational structure of the eight bands observed near the D 1 ← X 0^+ transition of KrXe

The rotational structure of the m, $m + 1$, $m + 2$ and $m + 3$ bands and of the *, **, *** and **** bands of KrXe measured by high-resolution (1+1′) resonant two-photon ionization spectroscopy are displayed in Figures 4 and 5, respectively. These spectra correspond to the $^{84}Kr^{136}Xe$ isotopomer except those of transitions to the *** and **** levels which could only be recorded with satisfactory signal-to-noise ratio for the main isotopomer $^{84}Kr^{132}Xe$.

All eight spectra consist of P, Q and R branches so that all vibrational levels belong to electronic states of $\Omega = 1$ symmetry. The analysis of combination differences further revealed that all eight transitions originate from the X 0^+ ($v'' = 0$) ground state.

The spectra presented in Figures 4 and 5 are compared to spectra calculated assuming that the rotational structures of the $\Omega = 1$ levels are not perturbed and can be described by the standard expression for $\Omega = 1$ states

$$\frac{E_{\rm rot}(v, J)}{hc} = B_v \left[J(J + 1) - \Omega^2\right] - D_v \left[J(J + 1) - \Omega^2\right]^2 \pm \frac{1}{2} q_v J(J + 1). \quad (3)$$

These calculations enabled us to recognize obvious perturbations of the rotational structure such as those, discussed in more detail in Subsection 4.3, affecting selected rotational levels of the $m + 2$ band. The positions of the unperturbed lines were then used to derive the origin $\tilde{\nu}_{v'0}$, the rotational constants (B), the centrifugal distortion constants (D) and the Ω-doubling constants (q) of the final levels in a least-squares-fit procedure. The ground-state rotational constant was kept fixed to the values determined in the analysis of the C 0^+ ← X 0^+ band system presented in Section 3. The values of the band origins and molecular constants determined in this manner for $^{84}Kr^{132}Xe$, $^{84}Kr^{134}Xe$ and $^{84}Kr^{136}Xe$ are summarized in Table 3.

The inclusion of an Ω-doubling constant was not necessary in the analysis of all levels, but the decreasing intensities, with increasing J' value, of Q-branch lines ($\Omega = 1$ levels of f symmetry) compared to R- and P-branch lines ($\Omega = 1$ levels of e symmetry) independently indicated a different overall behavior of e- and f-symmetry levels, and a perturbation affecting only the f levels, as will be discussed in the next subsection.

In the case of the $^{84}Kr^{134}Xe$ and $^{84}Kr^{136}Xe$ isotopomers, the low natural abundance (5.95 % and 5.05 %, respectively) and the resulting poorer signal-to-noise ratio of the weaker bands prevented the determination of several molecular constants.

The four $m+i$ (i = 0-3) bands and the bands * and ** have a similar rotational structure with a pronounced P-branch bandhead and Q- and R-branches extending toward higher wave numbers with increasing spacing between successive rotational lines. The *** and **** bands have a markedly different structure, with Q- and R-branch bandheads. These differences are reflected by the values of the rotational constants which are larger than B_0'' for the former six bands but smaller for the latter two (see Table 3). The *** and **** levels must therefore be weakly bound (or metastable levels) located close to a dissociation limit.

4.2. Hyperfine structure of the m + i (i = 0-3) vibrational levels

The spectra of the $m + i$ ($i = 0 - 3$) bands of the KrXe isotopomers containing ^{129}Xe and ^{83}Kr isotopes reveal additional structures caused by the hyperfine interaction. An example is given in Figure 6 which compares the (1+1′) resonant two-photon ionization spectra of the $m + 1$ band of ^{84}Kr^{129}Xe (panel (a)) and ^{84}Kr^{132}Xe (panel (b)). The hyperfine structure leads to a splitting of the transitions into $2I_{\mathrm{Xe}} + 1$ components (*i.e.*, doublets for ^{84}Kr^{129}Xe) that is most pronounced at low J' values. Although several KrXe isotopomers contain Kr or Xe with $I \neq 0$, the hyperfine structure could only be cleanly resolved and analyzed for the ^{84}Kr^{129}Xe isotopomer. The analysis, using the expressions

$$\left\langle J\Omega IF|h_\Omega \vec{I}\cdot\vec{J}_a|J'\Omega IF\right\rangle = h_\Omega\,(-1)^{I+J'+F+J-\Omega}\begin{Bmatrix} I & J' & F \\ J & I & 1\end{Bmatrix}\begin{pmatrix} J & 1 & J' \\ -\Omega & 0 & \Omega\end{pmatrix} \times [I(I+1)(2I+1)]^{1/2}\,[(2J'+1)(2J+1)]^{1/2}\,\Omega \tag{4}$$

and

$$I(J'F'\leftarrow JF) \propto \left[\{(2J'+1)(2J+1)(2F'+1)(2F+1)\}^{1/2} \times \begin{pmatrix} 1 & J & J' \\ \Omega'-\Omega & \Omega & -\Omega'\end{pmatrix}\begin{Bmatrix} 1 & J & J' \\ I & F' & F\end{Bmatrix}\right]^2 \tag{5}$$

presented in the context of the study of the C 1 state of ArXe in Ref. [19], led to the hyperfine coupling constants h_Ω listed in Table 3. These constants are compared in Figure 7 with the hyperfine coupling constants of the 6s and 6p states of Xe corresponding to the relevant dissociation asymptotes (see Table 2). The hyperfine coupling constants lie close to the value of the 6s[3/2]$_2$ state of Xe and midway between those of the 6p and 6s′[1/2]$_1$levels. The *, **, *** and **** bands of ^{84}Kr^{129}Xe were too weak for their hyperfine structures to be observed.

4.3. Perturbations of the energy level structure and of the intensity distribution

The spectra of KrXe in the vicinity of the D 1 $\leftarrow$ X 0^+ band system are subject to three distinct perturbations. The first one, recognizable even at low spectral resolution in Figure 1b, affects the positions of the vibrational levels without leading to strongly perturbed rotational structures. This perturbation must be a homogeneous ($\Delta\Omega = 0$) perturbation. Consequently, at least two $\Omega = 1$ states must be present in this spectral region.

The second perturbation is revealed by a rapid decrease of the intensity of Q-branch lines beyond $J \approx 10$ compared to the intensity of P- and R-branch lines of the same J' value and also to the calculated Q-branch line intensities. This effect is not equally pronounced in all bands: It is most easily observed in the $m + 2$ (Fig. 4c), $m + 3$ (Fig. 4d), * (Fig. 5a) and ** (Fig. 5b) bands and hardly noticeable in the m, $m + 1$, *** and **** bands. As explained in the context of the analysis of the C $1 \leftarrow$ X 0^+ band system of ArXe in Refs. [36, 19], Q-branch transitions terminate in $\Omega = 1$ levels of f symmetry, which correspond to the 1^- component. These levels must be predissociated by an 0^- electronic state (heterogeneous perturbation), which, according to Table 2, is likely to be the 0^- state associated with the $Kr(^1S_0)$ + Xe 6s′ $[1/2]^o_0$ dissociation limit. The predissociation mechanism is analogous to that operative in the C 1 state of ArXe (see Ref. [19]). The heterogeneous interaction responsible for the predissociation of the C state is weak, only affects the Q-branch lines, and has no detectable effect on their positions and widths within the sensitivity and resolution limits of our experiments.

The third perturbation is observed as a weak local irregularity of the P, Q and R branches of the $m+2$ band (Fig. 4c), which is displayed on an enlarged scale in Figure 8. The perturbation has its most striking effects on the R(7), Q(8) and P(9) lines, which are entirely missing from the experimental spectrum (vertical dashed lines in Figure 8). The same perturbation is also noticeable in the reduced intensities and blue shifts of the R(8), Q(9) and P(10) lines (dashed-dotted lines in Figure 8) and in the reduced intensities and red shifts of the R(6), Q(7) and P(8) lines (dotted lines in Figure 8). The perturbation thus equally affects the e- and f-symmetry components so that one can conclude that the rotational levels of the perturbing state occur in degenerate pairs of levels of opposite parity. This state must therefore have $|\Omega| \geq 1$ symmetry. The level shifts (blue for the $J' = 9$ and red for $J' = 7$) further indicate that the rotational constant of the perturbing level is smaller than that of the $m+2$ level, *i.e.,* $B_{\text{pert}} < 2.23 \cdot 10^{-2}\,\text{cm}^{-1}$. Finally, the fact that the most perturbed lines have the smallest intensities and that the perturbing levels are not observable in the spectrum demonstrate that the perturbing level is predissociative.

The very restricted set of levels - $J' = 7, 8$ and 9 - affected by the perturbation and the fact that the level shifts are of the same order of magnitude as the spectral linewidths of $\approx 0.015\,\text{cm}^{-1}$ prevented the distinction between a homogeneous perturbation with another $\Omega = 1$ state and a heterogeneous perturbation with an $\Omega = 2$ state.

To analyze the perturbation and derive information on the perturbing state, a two-state homogeneous perturbation model was used, described by the Hamiltonian matrix

$$\hat{H} = \left(\begin{array}{ccc|ccc} E^0_{1,J=1} & & & V_{12} & & \\ & E^0_{1,J=2} & & & V_{12} & \\ & & \cdots & & & \cdots \\ \hline V_{12} & & & E^0_{2,J=1} & & \\ & V_{12} & & & E^0_{2,J=2} & \\ & & \cdots & & & \cdots \end{array}\right), \tag{6}$$

where $E^0_{1,J}$ and $E^0_{2,J}$ represent the fictive, "unperturbed" positions of the rotational levels of the $m + 2$ level and the

perturbing level, respectively ($\Omega = 1$ for both states)

$$E^0_{J,1\,\mathrm{or}\,2} = T^0_{\mathrm{ev},1\,\mathrm{or}\,2} + B^0_{1\,\mathrm{or}\,2}\left[J(J+1) - \Omega^2\right], \tag{7}$$

and V_{12} is the matrix element coupling states of the same J value. Because the Ω doubling is not resolved and the perturbation appears to affect both parity components equally, we assumed that Eqs. (6) and (7) describe both *e*- and *f*-symmetry levels with the same molecular constants.

The entirely missing R(7), Q(8) and P(9) lines in the spectrum of $^{84}Kr^{132}Xe$ (see Fig. 8a) imply that the $J' = 8$ levels of the $m + 2$ and the perturbing states are almost exactly degenerate. Assuming exact degeneracy, the vibronic term value $T^0_{\mathrm{ev},2}$ of the perturbing level can be expressed as a function of the vibronic term value $T^0_{\mathrm{ev},1}$ of the $m + 2$ level and the rotational constants B^0_1 and B^0_2 as

$$T^0_{\mathrm{ev},2} = T^0_{\mathrm{ev},1} + 71 \cdot (B^0_1 - B^0_2). \tag{8}$$

In the analysis, we first determined $T^0_{\mathrm{ev},1}$ and B^0_1 from the positions of the lines of the $m + 2 \leftarrow$ X band that are not affected by the perturbation (see Table 3; $T^0_{\mathrm{ev},1} = \tilde{\nu}_{m+2,0}$ and $B^0_1 = B'_{m+2}$). The values $B^0_2 = 0.02133(86)\,\mathrm{cm}^{-1}$ and $|V_{12}| = 0.011(5)\,\mathrm{cm}^{-1}$ were then obtained from the positions of the $J' = 7$ and 9 levels, from which the vibronic term value of the perturbing level can be estimated to be $77318.47\,\mathrm{cm}^{-1}$.

The second calculated spectrum (trace c)) in Fig. 8, presented below the experimental spectrum, was obtained by including the effects of the perturbation on the line positions, but disregarding its effects on the line intensities. Comparing all three spectra in Fig. 8 leads to the conclusion that the perturbation model based on Eqs. (6) and (7) adequately describes the positions of all lines affected by the perturbation which do not overlap with other transitions, *i.e.,* P(10), Q(9), R(8) and R(6).

The same perturbation was also observed in the spectra of the $m + 2 \leftarrow$ X 0^+ band of the $^{84}Kr^{134}Xe$ and $^{84}Kr^{136}Xe$ isotopomers, but was found to be centered halfway between the $J' = 7$ and 8 levels, and very close to the position of the $J' = 7$ level, respectively. The overlap of several transitions in the spectra of these isotopomers in the region of interest, however, hindered an unambiguous analysis. This observation, nevertheless, suggests that the isotopic shifts of the vibronic energy of the perturbing level are only slightly smaller than for the $m+2$ level, which, in turn, indicates that the perturbing level is a vibrationally excited level.

The analysis of the perturbation of the rotational structure of the $m + 2$ level leads to the conclusions that (i) the perturbation is extremely weak, (ii) it equally affects *e*- and *f*-symmetry levels, and (iii) the perturbing level is a predissociative level of $\Omega = 1$ or $\Omega = 2$ symmetry with slightly smaller rotational constants and isotopic shifts than the $m + 2$ level. The perturbation could also adequately be modeled by assuming a heterogeneous perturbation with a coupling element proportional to J' in Eq. (6). Unfortunately, the very small number of perturbed rotational levels did not allow us to draw any conclusions concerning a possible J' dependence of the coupling element that would prove or disprove the heterogeneous/homogeneous nature of the perturbation.

4.4. Discussion of the observed structure of the $\Omega = 1$ levels

Panels (a) and (b) of Figure 9 provide an overview of the rotational constants and vibronic term values determined experimentally for the eight observed $\Omega = 1$ levels of $^{84}Kr^{132}Xe$ (circles), $^{84}Kr^{134}Xe$ (squares) and$^{84}Kr^{136}Xe$ (triangles). The isotopic shifts of the $^{84}Kr^{134}Xe$ levels with respect to those of the $^{84}Kr^{132}Xe$ levels are displayed in panel (c). The band index used in Figure 9 runs from 1 to 8 in order of increasing excited-state energy.

The overall structure of the vibrational levels of $\Omega = 1$ symmetry and the irregular evolution with band index of the data presented in Figure 9 are indicative of the presence of at least two $\Omega = 1$ electronic states in the spectral region investigated.

The spectroscopic data summarized in Table 3 and Figure 9 provide a basis for a classification of the observed $\Omega = 1$ levels in terms of contributions from different electronic states. The classification of the $\Omega = 1$ levels in two groups (the levels labeled with $v = m + \Delta m$ ($\Delta m = 0 - 3$) and those labeled with asterisks, see Figure 1b) used so far was made on the basis of their intensities only. The rotational constants of the eight levels presented in Table 3 and Figure 9a) do not provide much supporting evidence for this classification. The levels labeled with *** and **** behave very differently from those labeled with * and **, and the evolution of the B values in the m-series, though indicating an overall decreasing trend with increasing Δm value, are too irregular.

As in the analysis of the C 1 state of ArXe, the reduced isotopic shifts

$$\frac{\Delta\tilde{\nu}^i}{(\rho_i - 1)} = \frac{1}{hc}\frac{\left(E^i(v') - E^{\rm ref}(v')\right)}{(\rho_i - 1)} \tag{9}$$

turned out to provide useful information. However, in the absence of a scheme enabling some sort of classification of the levels as successive members of specific progressions, a graphical representation of the reduced isotopic shifts as presented in Figure 6f of Ref. [19] for ArXe cannot be made in the present case. Plotting the reduced isotopic shifts (or the isotopic shifts as in Figure 9c)) of the bands as a function of an index running from 1 to 8 for the eight observed levels in order of increasing energy is problematic given the presence of at least two overlapping states. We therefore also plotted the reduced isotopic shifts as a function of the distance $\left\langle \frac{1}{R^2} \right\rangle^{-1/2}$ corresponding to the inverse square root of the rotational constant. The reason for such a choice is that this distance is expected to increase smoothly within the different progressions and therefore to naturally separate the different progressions. The resulting plot is presented in Figure 10, which also contains, in the upper panel, a plot of the band centers against $\left\langle \frac{1}{R^2} \right\rangle^{-1/2}$.

Whereas the upper panel of Figure 10 suggests a possible classification of the levels in two progressions, one consisting of the levels **, *** and ****, the other of the levels *, m, $m + 1$, $m + 2$ and $m + 3$, the reduced isotopic shifts depicted in the lower panel suggest a classification in four distinct groups, the first group (see dashed line) consisting of the levels * and **, the second (see dotted line) of the levels $m + 1$, $m + 2$ and $m + 3$, the third of the levels *** and ****, and the fourth of the level m. The attribution of these groups of levels to specific $\Omega = 1$ states is not straightforward and the discussion presented below must be considered as speculative.

The first group of levels (* and **) is characterized by large isotopic shifts. The levels * and ** are separated by $\sim$61.4 cm^{-1} and have the highest rotational constants of all $\Omega = 1$ levels observed. If these two levels are successive

members of the same vibrational progression, they must be excited vibrational levels of a strongly bound $\Omega = 1$ state. Considering the level correlations presented in Table 2, a possible assignment could then be a Rydberg state with [X 1/2]6pσ character correlating with the Kr(^{1}S$_0$) + Xe 6p[5/2]$_2$ dissociation limit at 78270 cm^{-1}.

The second group of levels ($m + 1$, $m + 2$, $m + 3$) is characterized by smaller reduced isotopic shifts, vibrational spacings in the range 10-12 cm^{-1} and by rotational constants similar to those estimated for low vibrational levels of the [A$_2$ 1/2] KrXe$^+$ ion-core levels using the potential curves reported in Ref. [9]. These levels must be relatively low vibrational levels of a weakly bound Rydberg state and the correlations in Table 2 suggest, as possible assignment, a Rydberg state of A$_2$[1/2]6sσ character associated with the Kr(^{1}S$_0$) + Xe 6s′[1/2]$^o_1$ dissociation limit at 77335 cm^{-1}. On the basis of the investigation of the C 1 level of ArXe citepiticco12a, one would expect such a level to have a potential hump separating the main well from the region of large internuclear distances near dissociation. The magnitude of the isotopic shifts of the three levels suggest that the vibrational quantum number of the $m + 1$ level is either 2 or 3.

The third group of levels (*** and ****) is characterized by small reduced isotopic shifts, which even decrease with increasing $\left\langle \frac{1}{R^2} \right\rangle^{-1/2}$ value. Their spacing is very small (~7.1 cm^{-1}) and their rotational constants are the smallest of all $\Omega = 1$ levels observed. These levels must be levels located close to a dissociation limit which, on the basis of the band centers, can only be the Kr(^{1}S$_0$) + Xe 6s′[1/2]$^o_1$ dissociation limit at 77335 cm^{-1}. Their positions lie 12 cm^{-1} and 19 cm^{-1} above this limit so that these levels must be metastable resonances located near a local maximum on their potential energy curve. They may therefore be part of the same progression as those of the second group ($m + 1$, $m + 2$ and $m + 3$). The last level labeled m does not fit in any category. Its significant isotopic shift indicates that it is not a $v' = 0$ level. It is very difficult to find any, even very tentative assignment for this level. Its isolated nature suggests that it probably arises from a strong perturbation.

To test the tentative assignments made for the first two groups of levels, model calculations have been performed using the potential-energy functions $V_{\text{ion core}}(R)$ of the X 1/2 and A$_2$ 1/2 states of KrXe$^+$ from Ref. [9]. In the simplest calculations and to limit the number of adjustable parameters to only one per potential energy function, these ion-core potential-energy functions

$$V(R) = a \cdot V_{\text{ion core}}(R) + E_{\text{Diss}} \tag{10}$$

were scaled linearly (factor a in Eq. (10)) and shifted to the appropriate dissociation energies (77335 cm^{-1} for the $m + 1$, $m + 2$ and $m + 3$ progression, and 78270 cm^{-1} for the * and ** progression). In the case of the A$_2$ 1/2 potential energy function, an additional term

$$V_{\text{Rep}}(R) = C_{\text{Rep}} \int_{R-r_{\text{Kr}}}^{R+r_{\text{Kr}}} \frac{|\Psi_{\text{R}}(R)|^2}{R^2} \mathrm{d}R \tag{11}$$

was introduced to account for the overlap repulsion that takes place when a closed-shell atom is located near an amplitude maximum of the Rydberg electron wave function [12], and to test the hypothesis that the bands *** and **** belong to this progression. The form of this term was chosen so as to be consistent with our previous investigation of ArXe [19]. In Eq. (10), E_{Diss} corresponds to the position of the relevant dissociation limits relative to the X 0$^+$ (v

= 0) ground state of KrXe as explained above. In Eq. (11), $\Psi_R(R)$ is the radial part of the Rydberg electron wave function given by [37]

$$\frac{\Psi_R(R)}{R} = K \cdot W_{\kappa,l+1/2}\left(\frac{2R}{\kappa}\right), \tag{12}$$

where $K = \left[\kappa^2\Gamma(\kappa + l + 1)\Gamma(\kappa - l)\right]^{-1/2}$, $W_{\kappa,\mu}(z)$ is Whittaker's function [38], $\kappa \equiv n^* = n - \delta$, and δ is the quantum defect. A value of $r_{Kr} = 1.65$ Å [39] was used to evaluate Eq. (11).

The scaling factors a in Eq. (10) were then optimized so as to best reproduce the experimental positions of the relevant $\Omega = 1$ levels. The results of these simple calculations are presented in Table 4 where the rotational constants B_{calc} and the level positions $\tilde{\nu}_{calc}$ are compared with the experimental data. The optimal scaling factors are presented in Table 5. We have also added, in Table 4, the position and rotational constant calculated for the level of the second progression located below the $m + 1$ level to see how closely these values correspond to those observed for the level labeled 'm'. Deviations in the positions and the rotational constants are up to $\sim$2 cm^{-1} and 0.004 cm^{-1}, respectively, the largest deviations being for the levels **, $m + 2$ and $m + 3$. Not surprisingly, the position of the level labeled 'm' is not well described by the potential calculations. While overall encouraging, these calculations suffer from two main limitations: First, they do not account for the perturbed appearance of the experimental spectrum and second, the potential hump is not high enough (by $\sim$ 10 cm^{-1}) to account for the positions of the levels *** and ****. Whereas the second limitation does not really pose a problem for a qualitative understanding of the experimental observations (the height of the potential hump could be adjusted by introducing an additional fit parameter), overcoming the first limitation necessitates the inclusion of an interaction between the two states.

To this end, a coupling term between these two states was introduced in a second set of calculations. The ingredients of the model, which is inspired by the work of Stahel *et al.* [40], are diabatic potential energy functions $V^{d,}_{Rg,X}(R)$ for the [X 1/2]-core Rydberg state and $V^{d}_{Rg,A_2}(R)$ for the unperturbed D state and an R-independent electronic coupling term $V_{ee'}$ between the two states. In order to limit the number of adjustable parameters, we assumed that the potential energy functions of the [X 1/2]-core Rydberg state $V^{d,}_{Rg,X}(R)$ and of the [A_2 1/2]-core state $V^{d}_{Rg,A_2}(R)$ are identical to those described above by Eqs. (10)-(11).

The positions of the vibrational levels of the interacting states were calculated as described by Stahel *et al.* [40] in their analysis of the spectrum of molecular nitrogen, and briefly summarized in the following. The eigenvalues were obtained by diagonalizing a vibronic interaction matrix H with diagonal elements

$$H_{ev} = \left\langle \Psi^d_{ev}(R)|T_R + V^d_e(R)|\Psi^d_{ev}(R)\right\rangle_R \tag{13}$$

and off-diagonal elements

$$H_{ev,e'v'} = V_{ee'} S_{ev,e'v'} (1 - \delta_{ee'}) \tag{14}$$

consisting of an R-independent interaction strength $V_{ee'}$ and a vibrational overlap integral $S_{ev,e'v'} = \left\langle \Psi^d_{ev}|\Psi^d_{e'v'}\right\rangle$. In Eq. (13), T_R represents the kinetic energy and $V^d_e(R)$ the diabatic potential-energy function of unperturbed electronic states e with associated vibrational wave functions $\Psi^d_{ev}(R)$.

The "perturbed" rotational constants B'_k were calculated using [40]

$$B'_k = C_k^T B C_k, \tag{15}$$

where C_k represent the eigenvectors and B the rotational matrix with diagonal elements

$$B_{ev} = \left(\frac{h}{8\pi^2 c\mu}\right)\left\langle \Psi^d_{ev}|R^{-2}|\Psi^d_{ev}\right\rangle \tag{16}$$

and off-diagonal elements

$$B_{ev,e'v'} = \left(\frac{h}{8\pi^2 c\mu}\right)\left\langle \Psi^d_{ev}|R^{-2}|\Psi^d_{e'v'}\right\rangle \delta_{ee'}. \tag{17}$$

The results of these calculations are presented in the rows labeled $\tilde{\nu}_{\mathrm{calc}^{\mathrm{na}}}$ and $B_{\mathrm{calc}^{\mathrm{na}}}$ in Table 4 and appear to overcome some of the deficiencies of the first calculations. The diabatic potential energy-functions used in the calculations are depicted in Figure 12 and the potential parameters are listed in Table 5. The rotational constants, vibronic term values and isotopic shifts calculated using this interaction model are presented in the lower panels [d)-f)] of Figure 9, where they can be compared with the experimental results shown in panels a)-c).

The experimental spectrum is compared with a spectrum calculated on the basis of our coupling model in Figure 11. The positions of the experimental band centers derived from the analysis of the rotational structure are indicated by the vertical dashed lines. In the lower panel, the calculated positions of the levels with predominant '[X 1/2]-core' and '[A_2 1/2]-core' character are marked by open circles and squares, respectively. The calculated intensities, which correspond to the height of the thick vertical lines in the lower panel were obtained by assuming that the intensities exclusively originate from the '[A_2 1/2]-core' character of the coupled levels and is proportional to the Franck-Condon factors of the transitions from the X 0^+ ($v'' = 0$) ground-state levels to the vibrational levels of the [A_2 1/2]-type potential. The calculated intensities are in good qualitative agreement with the experimental ones, with the exception of the transition to the $m + 3$ [A_2 (5)] level which is too weak, and that of the [A_2 (1)] level, which is predicted to have a measurable intensity but has not been observed.

Whereas the calculated values of the rotational constants and vibronic term values of all levels except the level labeled 'm' are in good overall agreement with the experimental results (see panels a), b), d) and e) of Figure 9), the isotopic shifts are poorly described by the calculations. This discrepancy represents the main deficiency of our coupling model and precludes a definitive assignment of the observed spectral structures in terms of the potential energy functions depicted in Figure 12.

The results of our calculations presented in Table 5 and in Figs. 9 and 11, though promising, still fail to account for important aspects of the experimental data. Firstly, the position of the level labeled m remains poorly described. The calculations predict a level in its vicinity but not close enough (the deviation is $\sim 5\,\mathrm{cm}^{-1}$) for an unambiguous assignment. Secondly, the model does not account for the levels labeled *** and ****, although future improvements of the potential term (Eq. (11)) describing the local maximum of the potential energy function might overcome this deficiency. Finally, the investigation of the photoelectron and photoionization spectra of $KrXe^+$ from the D 1 state

reported in Ref. [9] indicate that the $m + 1$ level must also have [A_1 3/2] ion-core character next to the [X 1/2] and [A_2 1/2] character already included in our model. Given the restricted number of observed levels, it is not possible to include more electronic states in the model because the number of adjustable parameters would exceed the number of observed level positions.

The assignment of the bands labeled * and ** must be regarded as particularly tentative because there are multiple ways by which two levels of a deep potential well can be matched to two observed positions. *Ab initio* calculations of the electronically excited states of KrXe would be very valuable to improve the understanding of the $\Omega = 1$ levels observed in the present investigation.

5. Rotationally resolved PFI-ZEKE photoelectron spectra of the X 1/2 and A_1 3/2 states of $KrXe^+$

Compared to ArXe, the larger number of isotopomers of KrXe and the denser rovibrational energy level structure of the X 0^+, C 0^+ and D 1 states makes it much more difficult to select single rotational transitions of single isotopomers in the C ← X and D ← X band systems for the investigations of rovibronic photoionization dynamics by PFI-ZEKE photoelectron spectroscopy. The problem of spectral congestion is illustrated in Figure 2 which shows, with the example of the C 0^+ ($v' = 18$) ← X 0^+ ($v'' = 0$) transition, how the rotational structure of the different isotopomers overlap. The clean selection of single rovibrational levels of the intermediate state turned out not to be possible using the D ← X band system because of the additional Q-branch transitions in this $\Omega = 1 \leftarrow \Omega = 0$ perpendicular transition and their overlap with the P- and R-branch transitions (see, *e.g.,* Figure 4).

The C 0^+ ($v' = 19$) ← X 0^+ ($v'' = 0$) transition turned out to be best suited to the selection of individual rotational lines of selected isotopomers. PFI-ZEKE photoelectron spectra of the X 1/2 ($v^+ = 5, 22, 28$) states of $^{84}Kr^{132}Xe^+$ could be recorded from the C 0^+ ($v' = 19$) $J' = 8, 11, 12$ and 14 intermediate levels, and spectra of the A_1 3/2 ($v^+ = 3 - 5$) states of both $^{84}Kr^{132}Xe^+$ and $^{84}Kr^{129}Xe^+$ through the C 0^+ ($v' = 19$) $J' = 10, 12$ and 14 and C 0^+ ($v' = 19$) $J' = 8, 11$ and 13 intermediate levels, respectively. No spectra of sufficient quality could be recorded for the A_2 1/2 states of any isotopomer of $KrXe^+$, possibly because the C 0^+ state of $KrXe^+$ possesses less [A_2 1/2] ion core character than the D 0^+ state of ArXe.

To model the rotational intensity distributions, the same procedure as described for $ArXe^+$ in Ref. [20] was followed. The line positions of the X 1/2 state of $KrXe^+$ were evaluated using the expressions describing the coupling between $^2\Sigma^+_{1/2}$ and $^2\Pi$ states [41]

$$E(^2\Sigma^+; v^+, N^+, F_1)/hc = T^{(v^+)}_{\Lambda=0} + B^{(v^+)}_{\Lambda=0} N^+(N^+ + 1) + \frac{1}{2}\gamma^{(v^+)} N^+, \text{ for } J^+ = N^+ + 1/2 \quad (18)$$

$$E(^2\Sigma^+; v^+, N^+, F_2)/hc = T^{(v^+)}_{\Lambda=0} + B^{(v^+)}_{\Lambda=0} N^+(N^+ + 1) - \frac{1}{2}\gamma^{(v^+)}(N^+ + 1), \text{ for } J^+ = N^+ - 1/2 \quad (19)$$

and those of the A_1 3/2 state were derived from the effective Hamiltonian adapted to Hund's case (a) angular momentum coupling [42, 43, 44] (neglecting the Ω-doubling)

$$E_{\Omega=3/2}(v^+, J^+)/hc = T^{(v^+)}_{3/2} + B^{(v^+)}_{3/2}\left[J^+(J^+ + 1) - \tfrac{9}{2}\right]. \quad (20)$$

The line intensities were estimated following the same procedure as reported for $ArXe^+$ which relies on the photoionization selection rules

$$\Delta J = J^+ - J = -l - 3/2, -l - 1/2, \ldots, l + 3/2 \tag{21}$$

and

$$\begin{aligned} + \leftrightarrow +, - \leftrightarrow -, + \nleftrightarrow - \text{ for } \; l \text{ odd} \\ + \leftrightarrow -, + \nleftrightarrow +, - \nleftrightarrow - \text{ for } \; l \text{ even,} \end{aligned} \tag{22}$$

and Eqs. (7) and (8) of Ref. [20] for the relative intensities. The dominant partial waves were determined by assuming that the ionization process preserves the ion-core state, *e.g.*, that the X 1/2 and the A_1 3/2 states are accessed from the [X 1/2]6pσ and the [A_1 3/2]6pπ components of the C 0^+ state, respectively (see Table 2). Applying the atomic selection rules $\Delta l = \pm 1$ for the ionization step leads in both cases to dominant s and d partial waves, *i.e.*, even l values in Eqs. (21) and (22). However, the heteronuclear nature of KrXe and the fact that the center of mass and center of charge do not coincide inevitably leads to l mixing.

5.1. The X 1/2 ← C 0^+ photoelectron transition of KrXe

Figure 13 displays the PFI-ZEKE photoelectron spectra of the X 1/2 (5,22,28) ← C 0^+ ionizing transitions of $^{84}Kr^{132}Xe^+$. The structure of these spectra is similar to that observed in the X 1/2 ← D 0^+ transitions of ArXe (compare Figure 13 with Figure 9 of Ref. [20]), but the intensity distributions of spectra recorded from different intermediate levels to different ionic levels are overall more similar in KrXe than in ArXe. Moreover, the model calculations relying on the assumption that ionization takes place out of the [X 1/2]6pσ component are in better agreement with the experimental spectra in KrXe than in ArXe. These observations suggest that the contributions from direct ionization to the PFI-ZEKE photoelectron spectra are larger for KrXe than they are for ArXe and, consequently, that the C 0^+ state of KrXe has a stronger [X 1/2] ion-core character than the D 0^+ state of ArXe. This stronger [X 1/2] ion-core character is also likely to be one of the reasons for the fact that the C 0^+ state of KrXe is much more strongly bound ($D_e > 1000\,cm^{-1}$) than the D 0^+ state of ArXe ($D_e \approx 100\,cm^{-1}$ [19]).

None of the spectra displayed in Figure 13 reveals any obvious spin-rotation splittings. In the limit of a vanishing spin-rotation coupling constant γ, each rotational level with rotational quantum number N is expected to consist of a pair of degenerate states of the same parity ($(-1)^{N^+ + 1}$) and $J = N \pm 1/2$. Because the photoelectron spectra are obtained from a single rotational level of the intermediate state with a well-defined parity, the parity selection rule (Eq. (22)) would in this case inevitably give rise to an alternation of intensities between transitions to states of even and odd N^+ values. However, no obvious alternation of intensities between successive rotational lines can be detected within the resolution and sensitivity limits of our measurements. Instead, the photoelectron spectra are characterized by a rather smooth intensity variation over the entire rotational profile. We therefore conclude that the rotational energy levels form pairs of levels of *opposite* parity, as depicted schematically in Figure 9c of Ref. [20], which implies that

$|\gamma| = 2B$. The X 1/2 state of $KrXe^+$, like the X 1/2 state of $ArXe^+$, thus also conforms to the single-perturber and pure precession, strong $^2\Pi - {}^2\Sigma$ coupling case, discussed in Section 5B of Ref. [20], for which the spin-rotation coupling constant $\gamma \approx -2B$. From this observation, we anticipate that the Λ (Ω) doubling constant of the A_2 1/2 state of $KrXe^+$ should also approximately be $p = -2B$.

The molecular constants $T^{v^+}_{\Lambda=0}$ and $B^{v^+}_{\Lambda=0}$ of the X 1/2 state of $KrXe^+$ obtained with this assumption are listed in Table 6. From these constants, we estimate the equilibrium internuclear separation of the X 1/2 state of $KrXe^+$ to be 3.06(18) Å.

5.2. The A_1 3/2 ← C 0^+ photoionizing transition of KrXe

The rotationally resolved PFI-ZEKE photoelectron spectra of the A_1 3/2 ($v^+ = 3 - 5$) ← C 0^+ ($v' = 19$) transitions of $^{84}Kr^{132}Xe$ and of the A_1 3/2 ($v^+ = 3, 4$) ← C 0^+ ($v' = 19$) transitions of $^{84}Kr^{129}Xe$ are displayed in Figures 14 and 15, respectively. The intensity distributions in these spectra are very similar to those observed in the PFI-ZEKE photoelectron spectra of the A_1 3/2 ($v^+ = 0 - 2$) ← D 0^+ ($v' = 1$) transitions of ArXe (see Figure 6 of Ref. [20]) and follow the $\Delta J = \pm 1/2, \pm 3/2$ propensity rule expected for ionization out of the [A_1 3/2]6pπ component of the C 0^+ state even better than in the case of the A_1 3/2 ← D 0^+ transition of ArXe.

This observation indicates that the $l = 0, 2$ [A_1 3/2] ionization channels are dominant in the single-photon ionization of the C 0^+ state of KrXe, and supports the conclusions reached in Section 3 that the C 0^+ state possesses a significant [A_1 3/2] ion-core character.

Table 7 summarizes the molecular constants derived for the A_1 3/2 state from the analysis of the rotational structure. In the analysis, we assumed the Λ (Ω) doubling to be negligible, as expected for a $^2\Pi_{3/2}$ ($\Omega = 3/2$) state.

The equilibrium internuclear distance [$R_e = 3.71(66)$ Å] estimated from the rotational constants of the A_1 3/2 state and their v dependence lie halfway between the value obtained *ab initio* by Viehland *et al.* [45] and that of the semi-empirical potential functions determined in Ref. [9]. Given that our new experimental data confirms the vibrational assignments proposed in Ref. [9], they also confirm the values of the dissociation energies of the X 1/2 and A_1 3/2 states determined in Ref. [9] which differ from the values determined *ab initio*, as already noted by Viehland *et al.* [45].

6. Acknowledgments

We thank Dr. M. Schäfer, ETH Zürich, for useful discussions. This work is supported financially by the Swiss National Science Foundation under Project number 200020-135342 and by the European Research Council advanced grant program under Project number 228286.

References

[1] D. E. Freeman, K. Yoshino, Y. Tanaka, J. Chem. Phys. 67 (1977) 3462–3481.

[2] M. C. Castex, J. Chem. Phys. 66 (1977) 3854–3865.
[3] A. Balakrishnan, W. J. Jones, C. G. Mahajan, B. P. Stoicheff, Chem. Phys. Lett. 155 (1989) 43–46.
[4] M. Tsuji, M. Tanaka, Y. Nishimura, Chem. Phys. Lett. 262 (1996) 349–354.
[5] P. M. Dehmer, S. T. Pratt, J. Chem. Phys. 77 (1982) 4804–4817.
[6] S. T. Pratt, P. M. Dehmer, J. L. Dehmer, J. Chem. Phys. 83 (1985) 5380–5390.
[7] D. M. Mao, X. K. Hu, Y. J. Shi, R. H. Lipson, Phys. Chem. Chem. Phys. 3 (2001) 4258–4261.
[8] D. M. Mao, X. K. Hu, S. S. Dimov, R. H. Lipson, J. Phys. B: At. Mol. Opt. Phys. 29 (1996) L89–L94.
[9] O. Zehnder, F. Merkt, Mol. Phys. 106 (2008) 1215–1226.
[10] M. A. Khodorkovskiĭ, A. A. Belyaeva, L. P. Rakcheeva, A. A. Pastor, P. Yu. Serdobintsev, N. A. Timofeev, I. A. Shevkunov, R. Hallin, K. Siegbahn, Opt. Spectrosc. 102 (2007) 834–841.
[11] M. A. Khodorkovskiĭ, A. A. Belyaeva, L. P. Rakcheeva, P. Yu. Serdobintsev, A. A. Pastor, A. S. Mel'nikov, N. A. Timofeev, R. Hallin, K. Siegbahn, Opt. Spectrosc. 104 (2008) 674–685.
[12] R. H. Lipson, R. W. Field, J. Chem. Phys. 110 (1999) 10653–10656.
[13] C. D. Pibel, K. Yamanouchi, J. Miyawaki, S. Tsuchiya, B. Rajaram, R. W. Field, J. Chem. Phys. 101 (1994) 10242–10251.
[14] T. Tsuchizawa, K. Yamanouchi, S. Tsuchiya, J. Chem. Phys. 92 (1990) 1560–1567.
[15] C. Y. Ng, P. W. Tiedemann, B. H. Mahan, Y. T. Lee, J. Chem. Phys. 66 (1977) 5737–5743.
[16] H. Yoshii, T. Tanaka, Y. Morioka, T. Hayaishi, K. Ito, J. Chem. Phys. 111 (1999) 10595–10601.
[17] S. T. Pratt, P. M. Dehmer, J. L. Dehmer, Chem. Phys. Lett. 116 (1985) 245–249.
[18] O. Zehnder, F. Merkt, J. Chem. Phys. 128 (2008) 014306.
[19] L. Piticco, M. Schäfer, F. Merkt, J. Chem. Phys. 136 (2012) 074304.
[20] L. Piticco, F. Merkt, J. Chem. Phys. 137 (2012) 094308–94321.
[21] N. Y. Du, C. H. Greene, J. Chem. Phys. 90 (1989) 6347–6360.
[22] C. Jonin, P. Laporte, F. Spiegelmann, J. Chem. Phys. 117 (2002) 3049–3058.
[23] C. Jonin, F. Spiegelmann, J. Chem. Phys. 117 (2002) 3059–3073.
[24] I. Kopp, J. T. Hougen, Can. J. Phys. 45 (1967) 2581–2596.
[25] J. T. Hougen, J. Mol. Spectrosc. 42 (1972) 381–384.
[26] I. Dabrowski, G. Herzberg, K. Yoshino, J. Mol. Spectrosc. 89 (1981) 491–510.
[27] A. Carrington, T. P. Softley, Chem. Phys. 92 (1985) 199–219.
[28] U. Hollenstein, H. Palm, F. Merkt, Rev. Sci. Instr. 71 (2000) 4023–4028.
[29] R. Seiler, U. Hollenstein, G. M. Greetham, F. Merkt, Chem. Phys. Lett. 346 (2001) 201–208.
[30] G. Reiser, W. Habenicht, K. Müller-Dethlefs, E. W. Schlag, Chem. Phys. Lett. 152 (1988) 119–123.
[31] U. Hollenstein, R. Seiler, H. Schmutz, M. Andrist, F. Merkt, J. Chem. Phys. 115 (2001) 5461–5469.
[32] E. R. Cohen, T. Cvitaš, J. G. Frey, B. Holmström, K. Kuchitsu, R. Marquardt, I. Mills, F. Pavese, M. Quack, J. Stohner, H. L. Strauss, M. Takami, A. J. Thor, Quantities, Units and Symbols in Physical Chemistry, RSCPublishing, Cambridge, 3rd edition, 2007.
[33] W. Jäger, Y. Xu, M. C. L. Gerry, J. Chem. Phys. 99 (1993) 919–927.
[34] G. Herzberg, Molecular Spectra and Molecular Structure, Volume I, Spectra of Diatomic Molecules, Van Nostrand Reinhold Company, New York, 2nd edition, 1950.
[35] A. Hansson, J. K. G. Watson, J. Mol. Spectrosc. 233 (2005) 169–173.
[36] S. Liu, A. Hishikawa, K. Yamanouchi, J. Chem. Phys. 108 (1998) 5330–5337.
[37] M. J. Seaton, Proc. Phys. Soc. 88 (1966) 801–814.
[38] M. Abramowitz, I. A. Stegun (Eds.), Handbook of Mathematical Functions, Dover Publications, London, ninth edition, 1970.
[39] Y. Zhang, Zh. Xu, American Mineralogist 80 (1995) 670–675.
[40] D. Stahel, M. Leoni, K. Dressler, J. Chem. Phys. 79 (1983) 2541–2558.

[41] H. Lefebvre-Brion, R. W. Field, The Spectra and Dynamics of Diatomic Molecules, Elsevier, Amsterdam, 2004.

[42] L. Veseth, J. Phys. B: At. Mol. Phys. 6 (1973) 1473–1483.

[43] P. Rupper, F. Merkt, J. Chem. Phys. 117 (2002) 4264–4281.

[44] K. Vasilatou, U. Hollenstein, F. Merkt, Mol. Phys. 108 (2010) 915–926.

[45] L. A. Viehland, B. R. Gray, T. G. Wright, Mol. Phys. 108 (2010) 547–555.

[46] M. Schäfer, M. Raunhardt, F. Merkt, Phys. Rev. A 81 (2010) 032514.

[47] G. D'Amico, G. Pesce, A. Sasso, Phys. Rev. A 60 (1999) 4409–4416.

[48] D. A. Jackson, M. C. Coulombe, Proc. R. Soc. London A 335 (1973) 127–140.

[49] J. E. Sansonetti, W. C. Martin, J. Phys. Chem. Ref. Data 34 (2005) 1559–2259.

[50] K. T. Tang, J. P. Toennies, J. Chem. Phys. 118 (2003) 4976–4983.

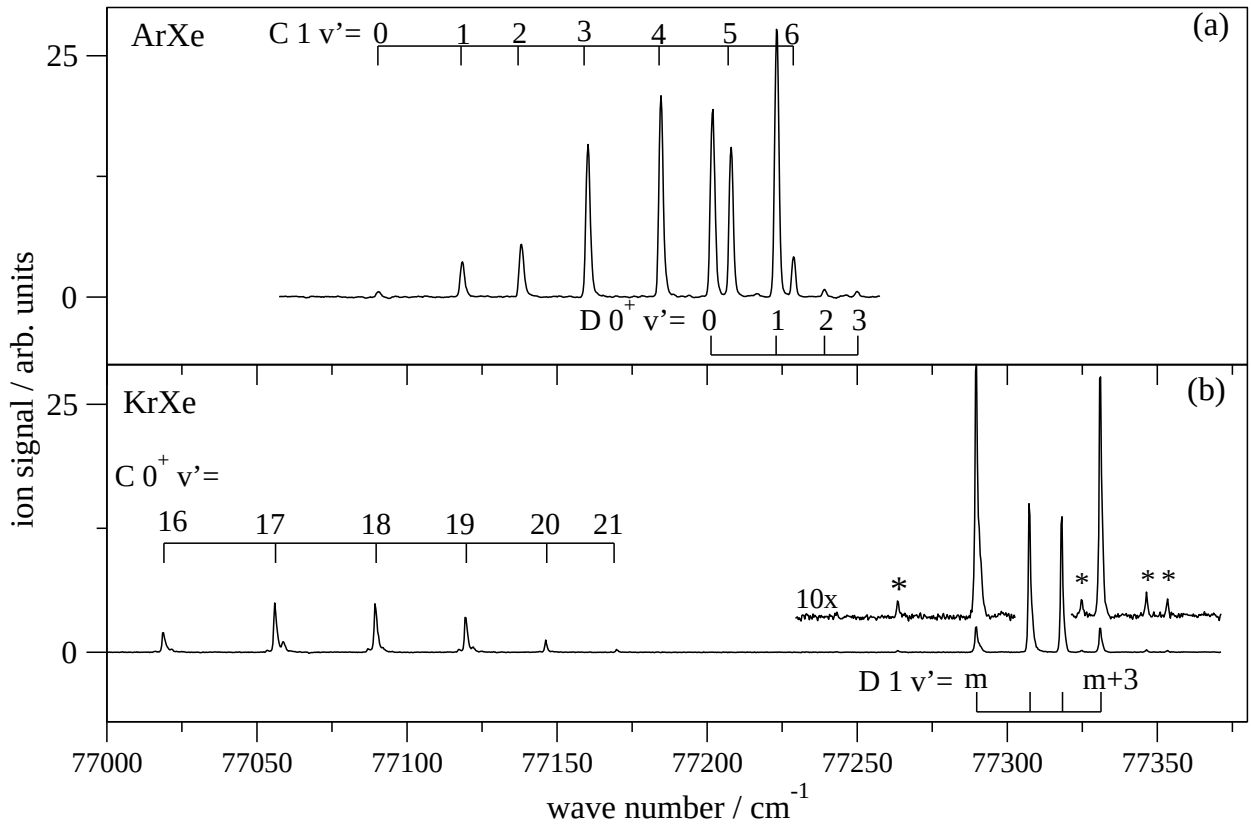

Figure 1: Vibrationally resolved REMPI spectra of the C and D Rydberg states of ArXe and KrXe in the vicinity of the Xe*($5p^5 6s'[1/2]^o_1$) + Rg($^1S_0$) (Rg=Ar,Kr) dissociation limits adapted from Refs. [18, 9]. (a) REMPI spectra of the C 1 ($v' = 0 - 6$) ← X 0^+ and D 0^+ ($v' = 0 - 3$) ← X 0^+ transitions of $Ar^{129}Xe$. (b) REMPI spectra of the C 0^+ ($v' = 16 - 21$) ← X 0^+ and D 1 ($v' = m - (m + 3)$) ← X 0^+ transitions of $^{84}Kr^{132}Xe$. The lines marked with asterisks represent lines that have remained unobserved or unassigned until the present investigation.

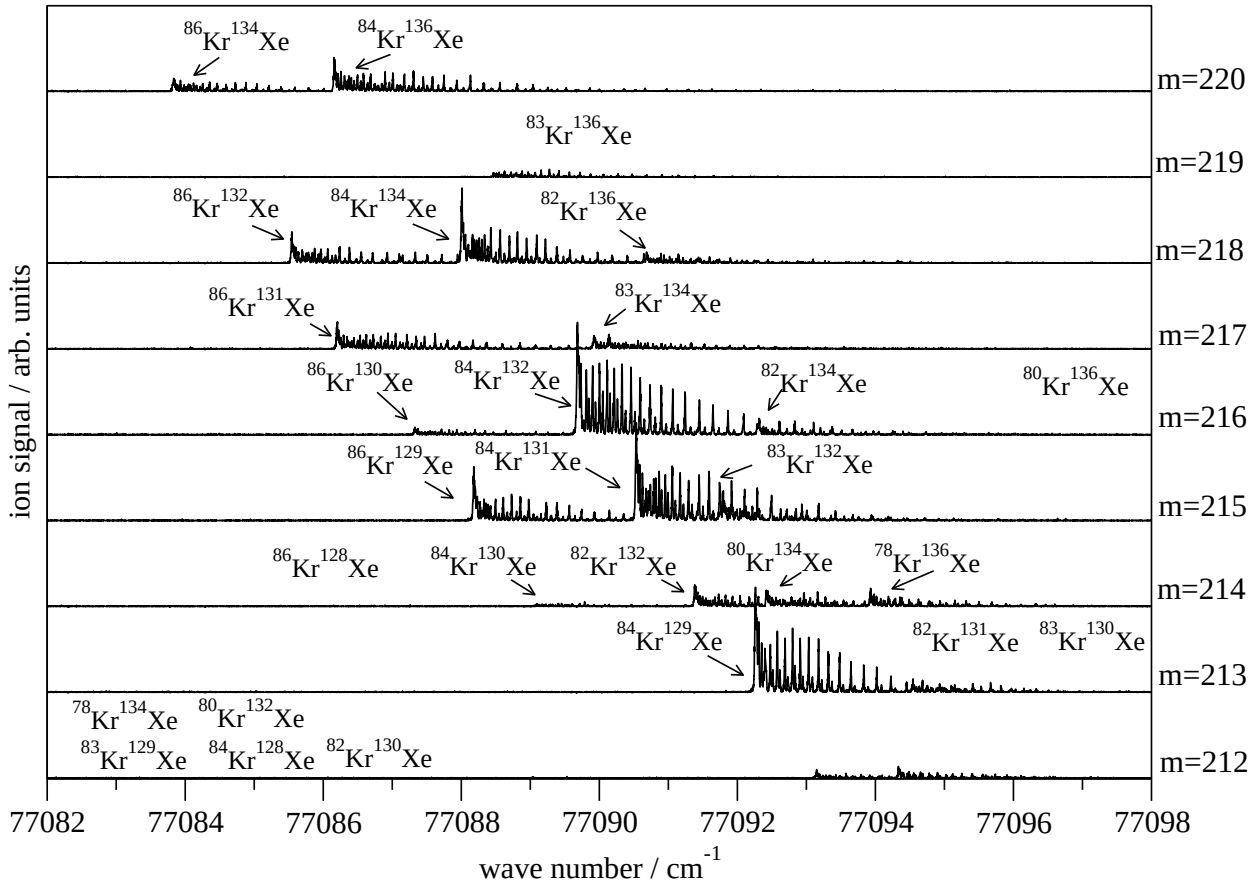

Figure 2: Rotationally resolved REMPI spectrum of the C 0^+ ($\nu' = 18$) ← X 0^+ transition of KrXe. The individual panels display the rotational structures of different isotopomers of the same mass number.

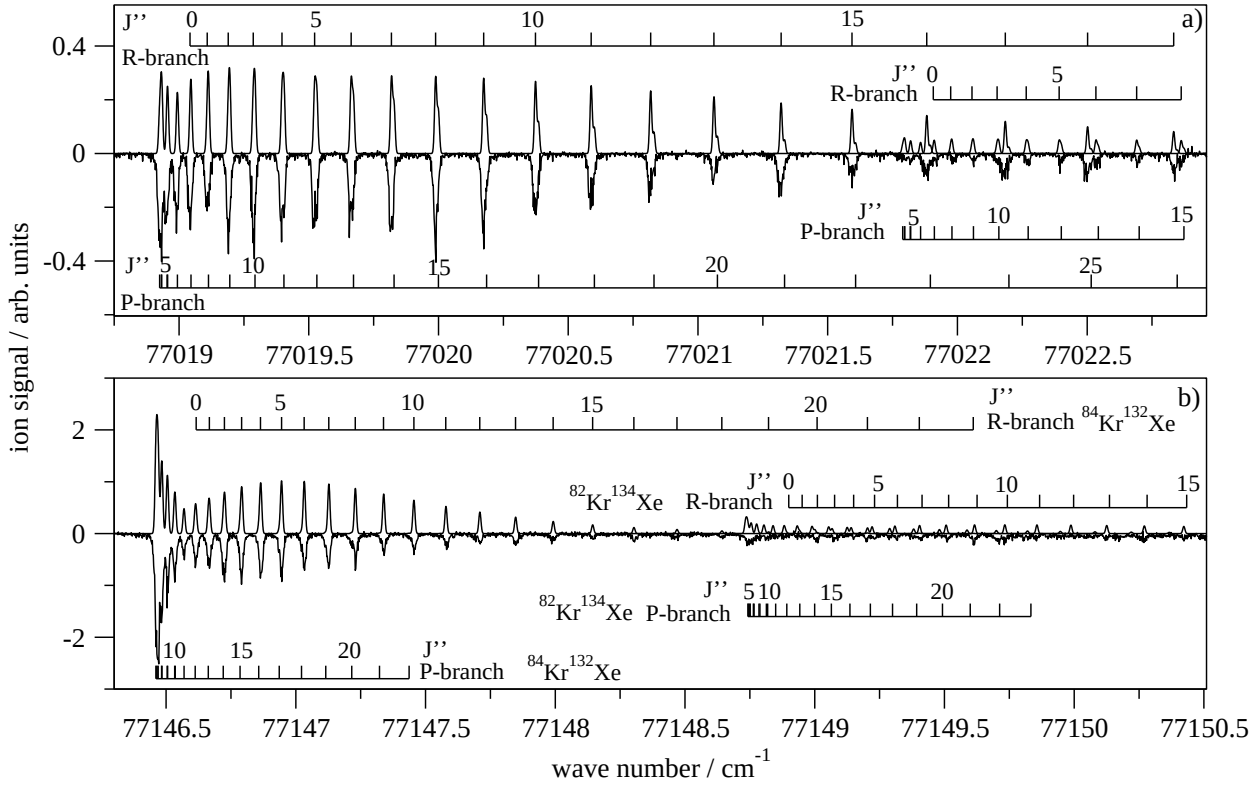

Figure 3: Rotationally resolved (1+1′) REMPI spectra of the C 0^+ (v' = 16) ← X 0^+ (panel (a)) and C 0^+ (v' = 20) ← X 0^+ (panel (b)) transitions of $^{84}Kr^{132}Xe$ and $^{82}Kr^{134}Xe$. In each panel, the experimental spectra are shown as lower, inverted traces, and the calculated spectra as upper traces. The assignment bars indicate the positions of the P- and R-branch transitions of both isotopomers.

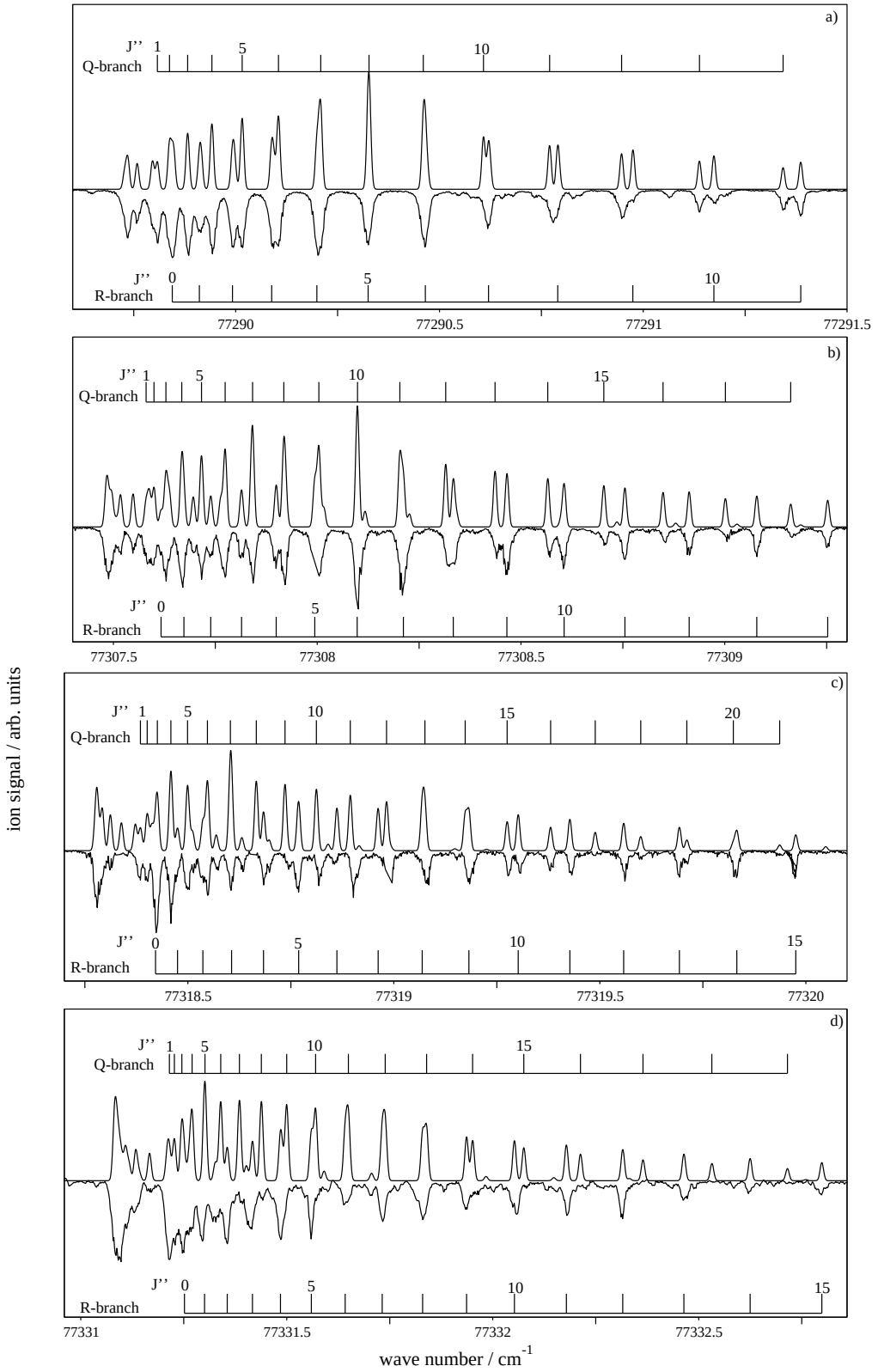

Figure 4: Rotationally resolved (1+1′) REMPI spectra of the D 1 (v') ← X 0^+ (v'' = 0) transitions of $^{84}Kr^{132}Xe$. (a) $v' = m$. (b) $v' = m + 1$. (c) $v' = m + 2$. (d) $v' = m + 3$. In each panel, the experimental spectra are shown as inverted traces and the calculated spectra as upper traces. The assignment bars on top of the calculated spectra indicate the positions of the Q-branch transitions and those below the experimental trace the positions of the R-branch transitions.

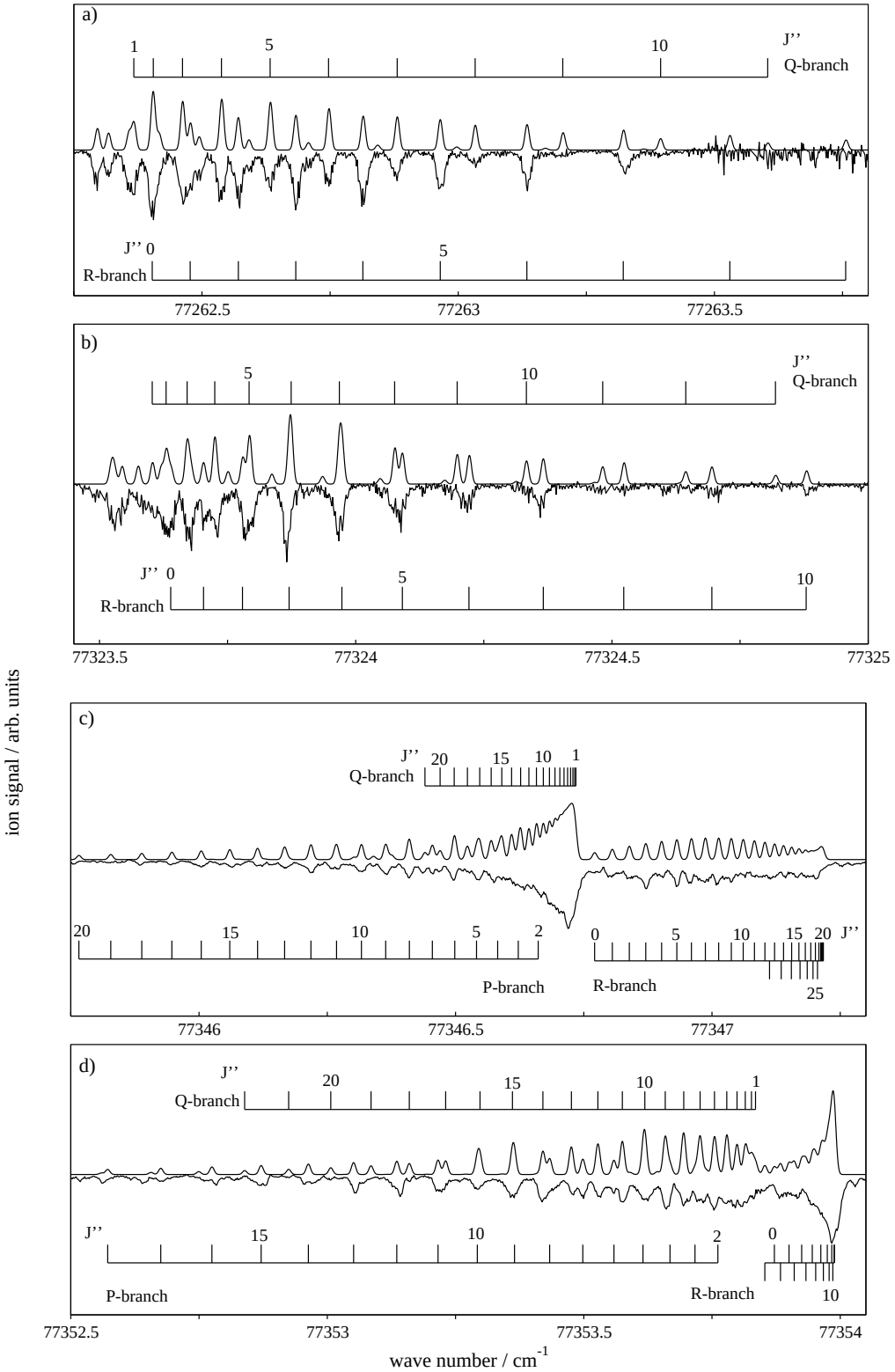

Figure 5: Rotationally resolved spectra of the $\Omega = 1$ (v^*, v^{**}) ← X 0^+ transitions of $^{84}Kr^{136}Xe$ (panel (a) and (b)) and of the $\Omega = 1$ (v^{***}, v^{****}) ← X 0^+ transitions of $^{84}Kr^{132}Xe$ (panel (c) and (d)). In each panel, the experimental spectra are shown as lower, inverted traces, and the calculated spectra as upper traces. The assignment bars indicate the positions of the P(J''), Q(J''), and R(J'') transitions.

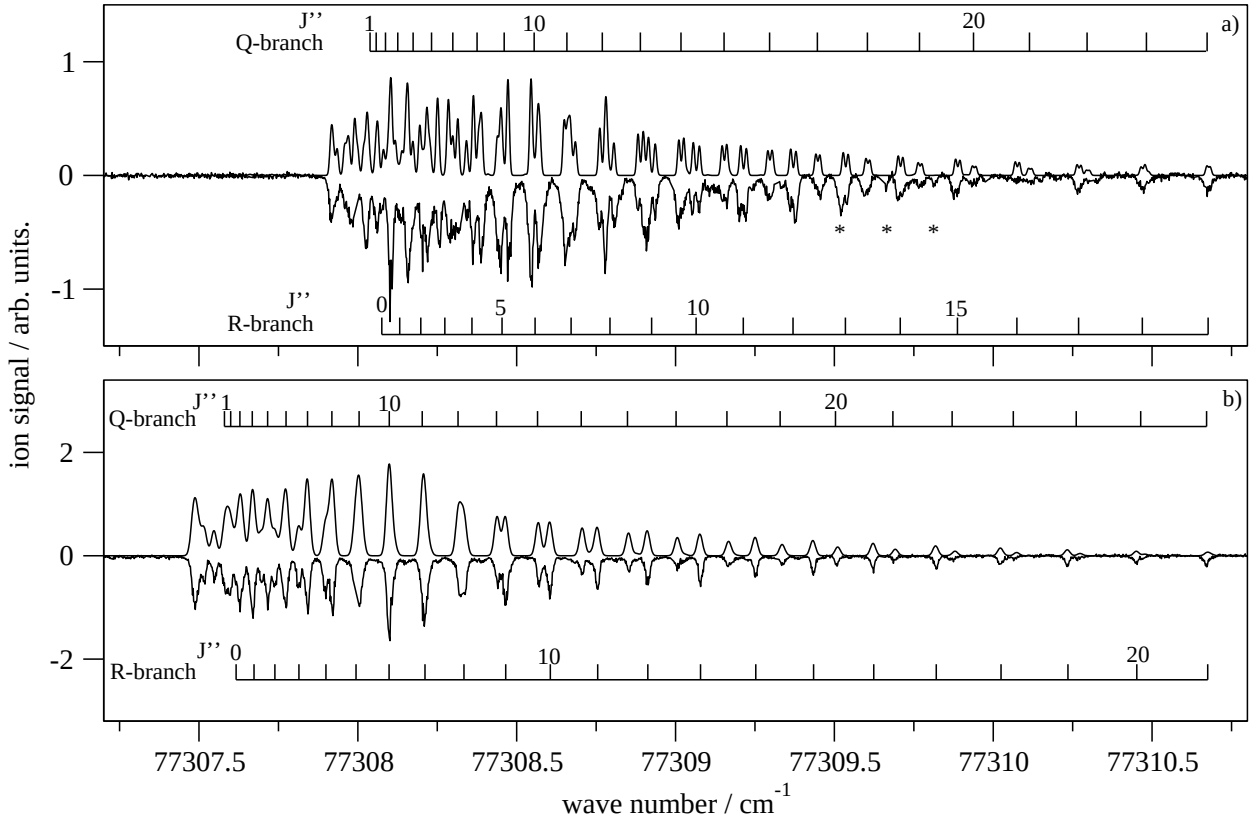

Figure 6: High-resolution (1+1′) REMPI spectrum of the D 1 ($v' = m + 1$) ← X 0^+ transitions of $^{84}Kr^{129}Xe$ (panel (a)) and $^{84}Kr^{132}Xe$ (panel (b)). In each panel, the experimental spectra are shown as lower, inverted traces, and the calculated spectra as upper traces. The asterisks designate D 1 ($v' = m + 1$) ← X 0^+ transitions of the $^{83}Kr^{130}Xe$ isotopomer.

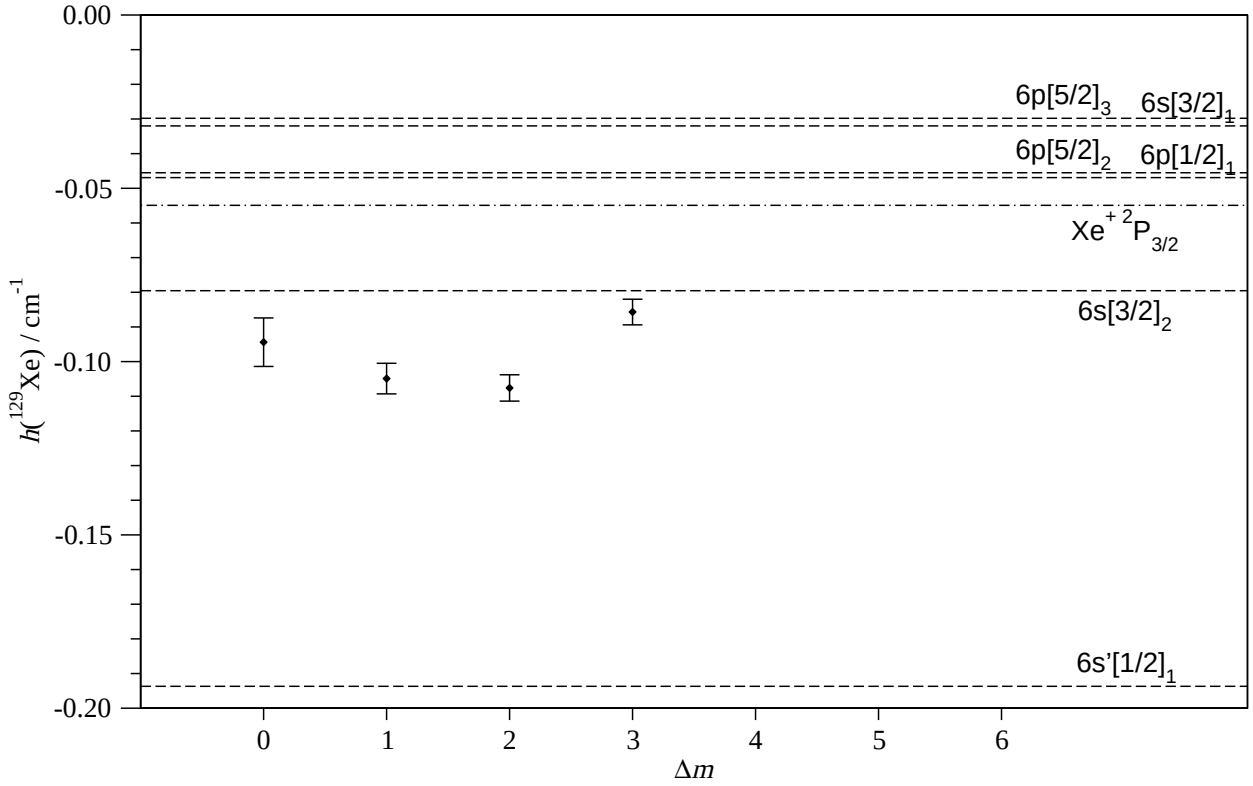

Figure 7: Comparison of the h_ν hyperfine-coupling parameters of the D 1 ($\nu' = m+\Delta m$) states of ^{84}Kr^{129}Xe with the corresponding magnetic-dipole hyperfine-coupling parameters of the relevant electronic states of Xe and Xe^+) [46, 47, 48].

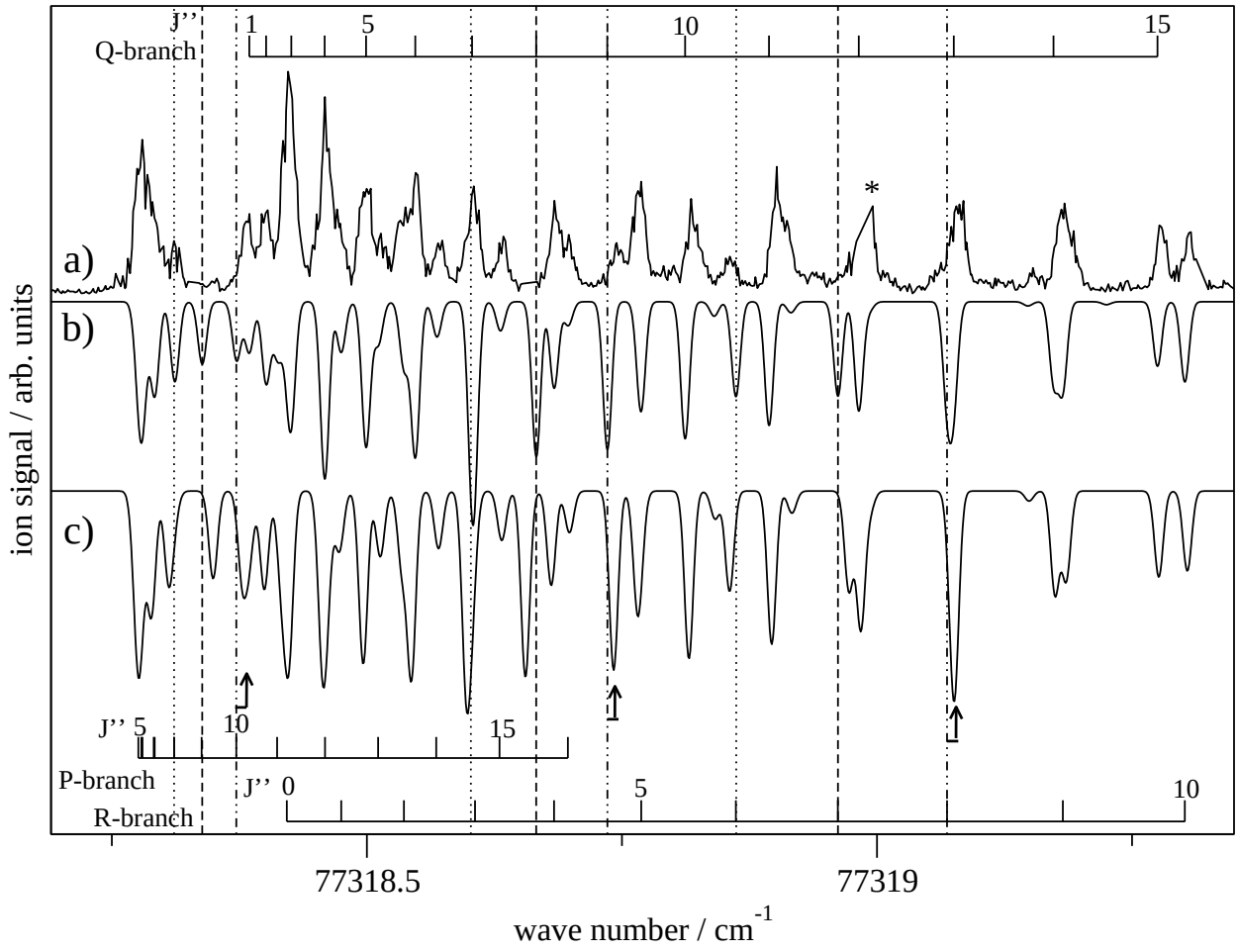

Figure 8: a) Rotationally resolved spectrum of the D 1 ($v' = m + 2$) ← X 0^+ transition of $^{84}Kr^{132}Xe$. The assignment bars indicate the positions of the P-, Q- and R-branch transitions. b) and c) Calculated spectra assuming no perturbation and with perturbation, respectively, are depicted as lower, inverted traces. The dashed lines indicate the calculated positions of the missing P(9), Q(8) and R(7) lines. The dashed-dotted and dotted lines indicate the calculated (unperturbed) positions of the P(10), Q(9) and R(8) lines and those of the P(8), Q(7) and R(6) lines, respectively. The line shifts resulting from the perturbation are best seen for the P(10), Q(9) and R(8) lines which do not overlap with other lines and are indicated by the arrows. The asterisk designates a region affected by a mode hop of the ring laser.

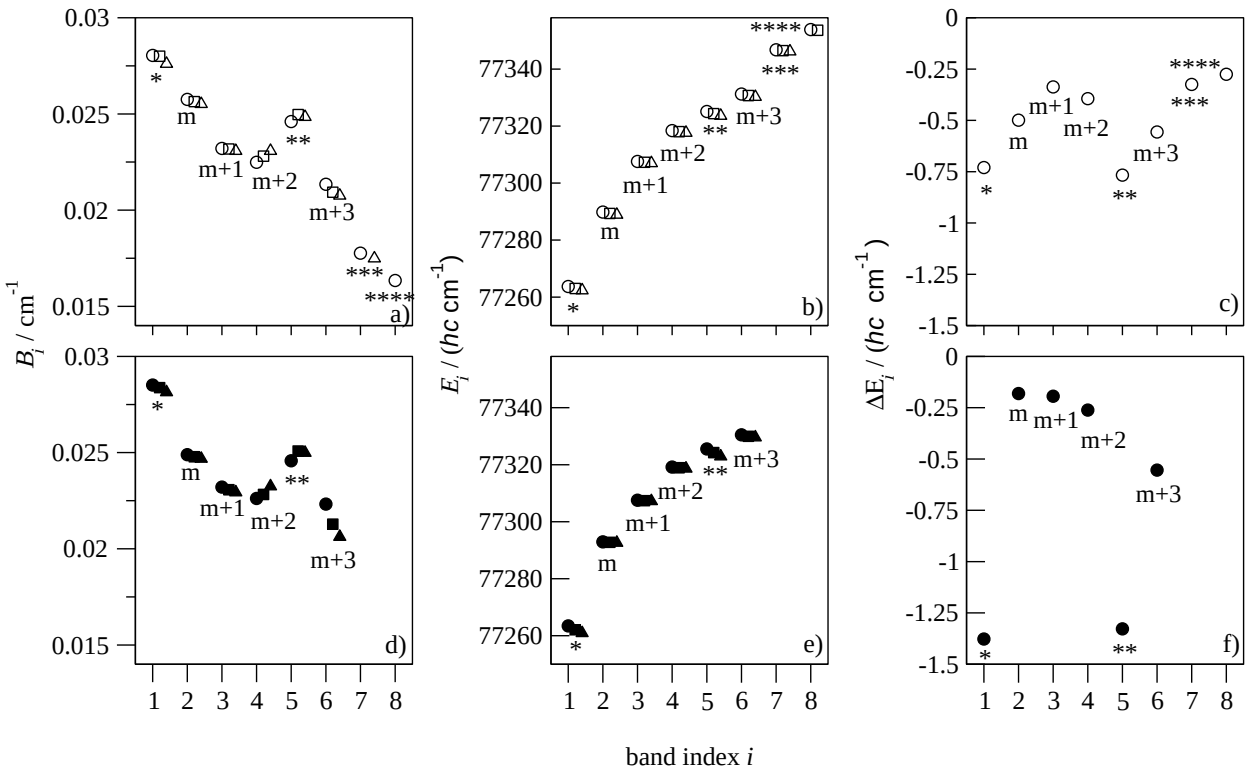

Figure 9: (a)-(b) Rotational constants and vibronic term values determined experimentally for the eight Ω = 1 levels of $^{84}Kr^{132}Xe$ (circles), $^{84}Kr^{134}Xe$ (squares) and $^{84}Kr^{136}Xe$ (triangles). The band index i=1-8 labels the vibrational levels in order of ascending energy. (c) Isotopic shifts of the band origins of $^{84}Kr^{134}Xe$ (corrected for the ground state isotope shifts, with $^{84}Kr^{132}Xe$ as reference isotopomer). d)-f) Rotational constants, vibronic term values and isotopic shifts calculated using our interaction model.

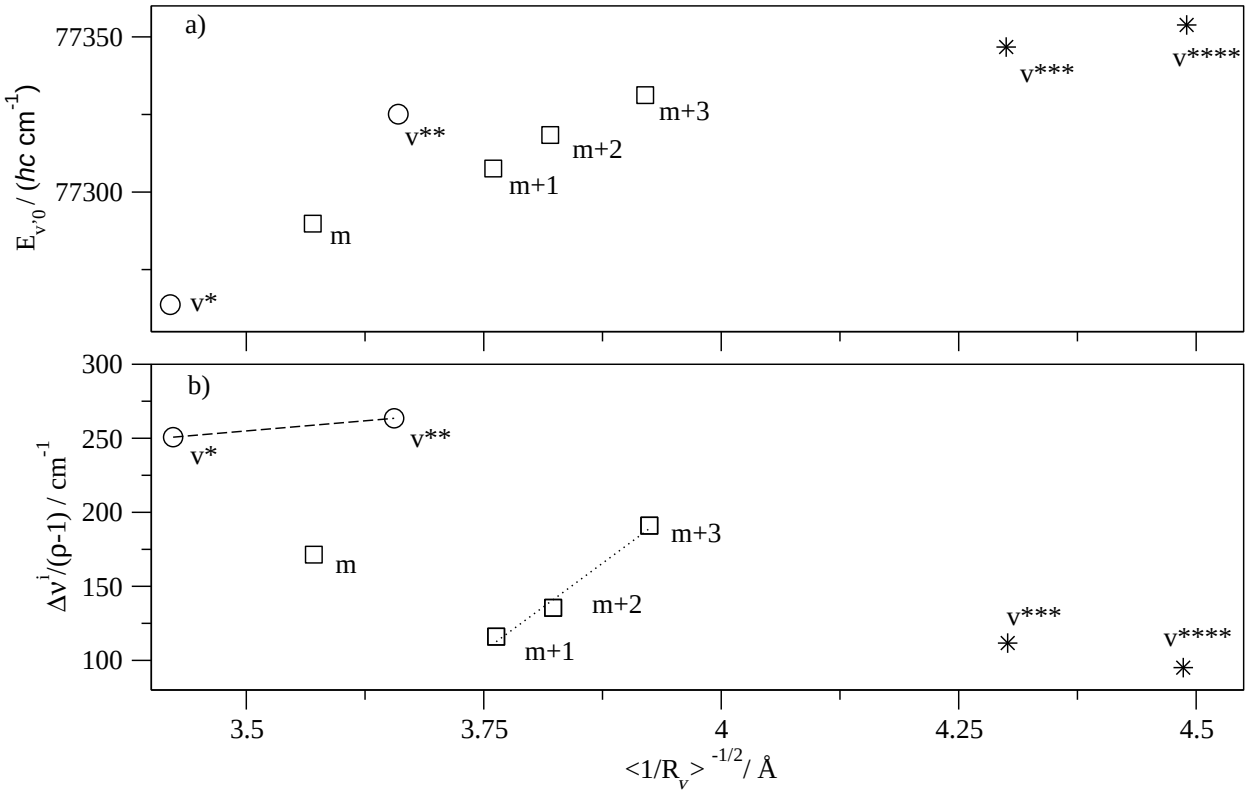

Figure 10: (a) Band origins of the $\Omega = 1$ (v^*, v^{**}) ← X 0^+ (circles), D 1 ($v' = m - (m + 3)$) ← X 0^+ (squares) and $\Omega = 1$ (v^{***}, v^{****}) ← X 0^+ (stars) transitions of $^{84}Kr^{132}Xe$ plotted against the distance $\left\langle \frac{1}{R^2} \right\rangle^{-1/2}$ corresponding to the inverse square root of the rotational constant. (b) Scaled isotopic shifts of the band origins of $^{84}Kr^{134}Xe$ (corrected for the ground state isotope shifts, with $^{84}Kr^{132}Xe$ as reference isotopomer) The dashed and dotted lines connect the levels * and ** and the levels $m + 1$, $m + 2$ and $m + 3$, respectively.

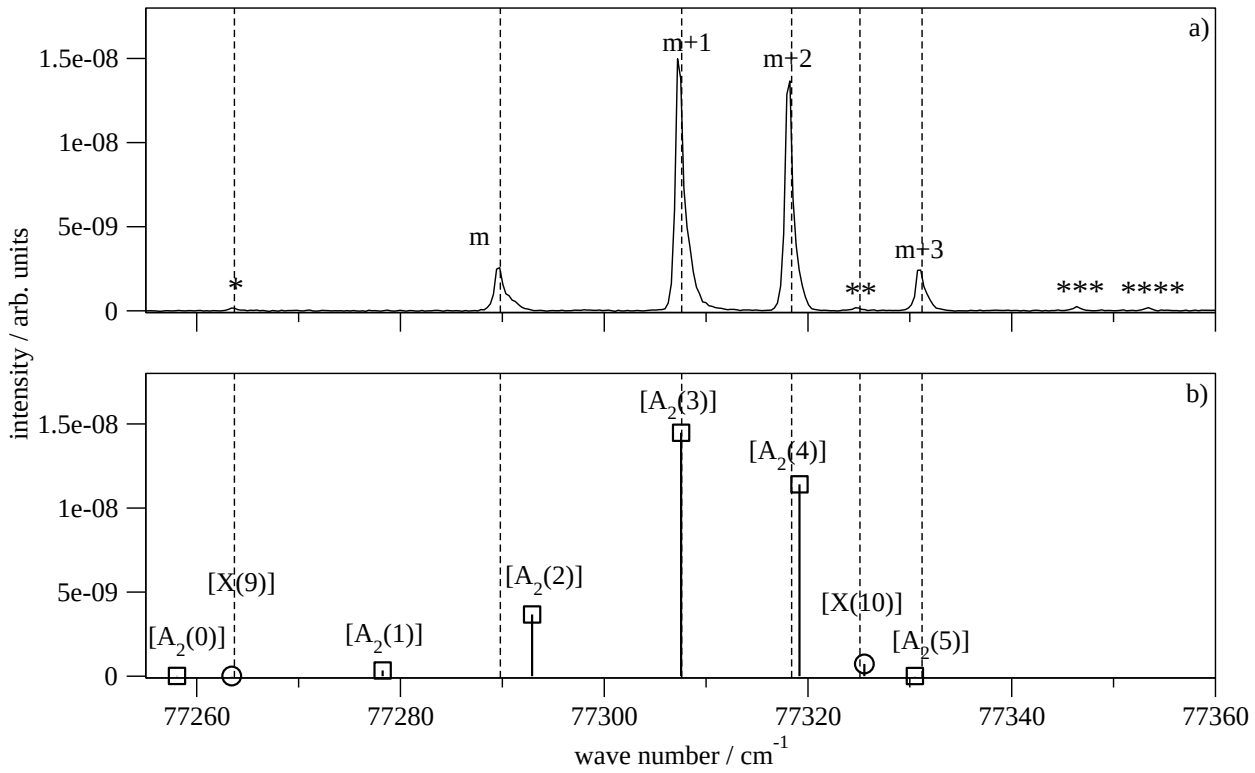

Figure 11: a) Vibrationally resolved REMPI spectrum of the D Rydberg state of KrXe in the vicinity of the $Xe^*(5p^5 6s'[1/2]^o_1) + Kr(^1S_0)$ dissociation limit adapted from Ref. [9]. b) Calculated positions of the levels with predominant [X 1/2]-core and [A_2 1/2]-core character, marked by circles and squares, respectively, determined from our interaction model. The dashed vertical lines in panels a) and b) indicate the experimental positions of the $v*$, $v**$ and $v = m + i$ ($i = 0 - 3$) vibrational levels, respectively.

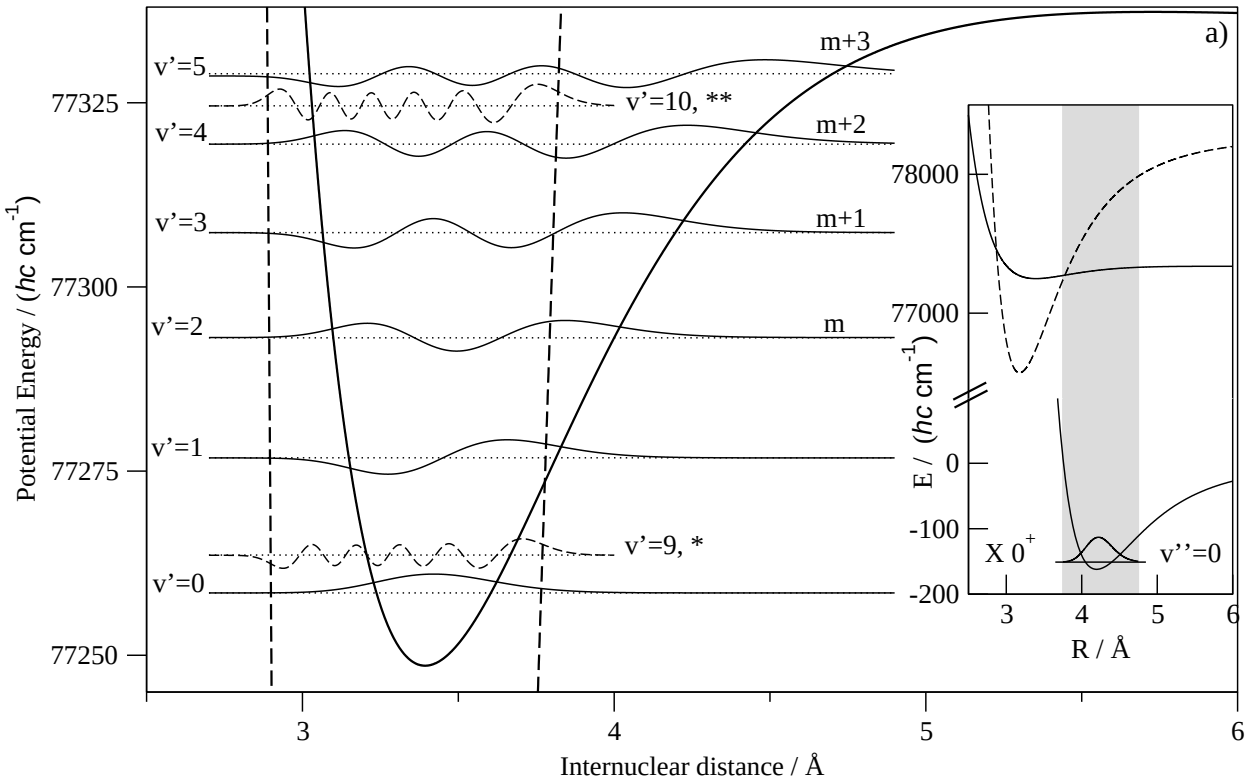

Figure 12: (a) Potential-energy functions of a Rydberg state with [X 1/2] core (dashed line) and [A_2 1/2] core (bold line) correlating with the Kr($^1S_0$) + Xe(6p[5/2]$_2$) and Xe(6s′[1/2]$^o_1$) dissociation limits, respectively. The energy positions and vibrational wavefunctions of the $v' = 0 - 5$ vibrational levels of the [A_2 1/2]-core Rydberg state and the $v' = 9, 10$ vibrational levels of the [X 1/2]-core Rydberg state visualize the effects of a perturbation most pronounced for [X 1/2] ($v' = 9$) ↔ [A_2 1/2] ($v' = 0$) and [X 1/2] ($v' = 10$) ↔ [A_2 1/2] ($v' = 4, 5$). Inset: The grey shaded area indicates the Franck-Condon region for excitation from the X 0^+ ($v'' = 0$) ground neutral state.

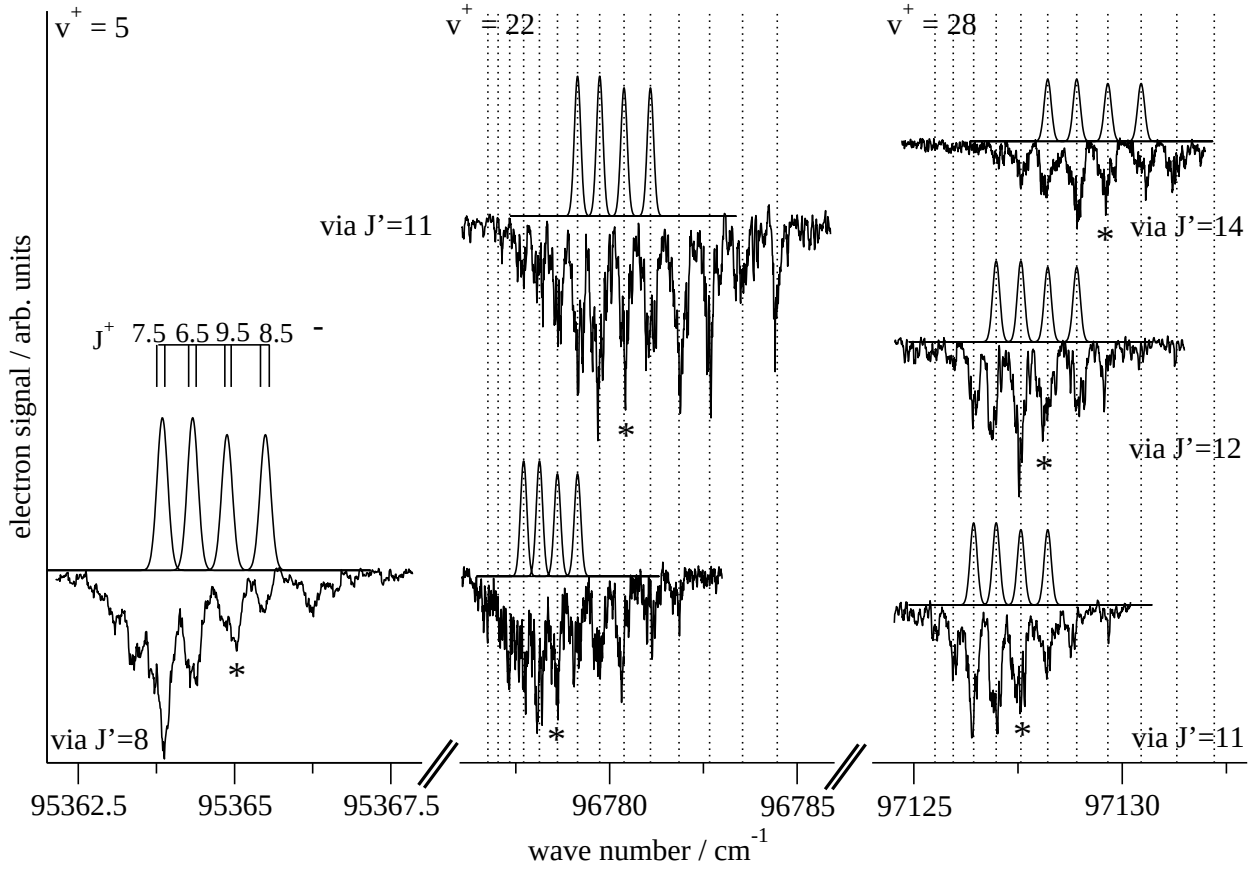

Figure 13: Rotationally resolved PFI-ZEKE photoelectron spectra of the $v^+ = 5, 22$ and 28 vibrational levels of the X 1/2 state of $^{84}Kr^{132}Xe$ recorded via the C 0^+ ($v' = 19, J' = 8, 11, 12, 14$) intermediate states. The experimental spectra are shown as lower, inverted traces and the calculated spectra as upper traces. The lines corresponding to the overlapping $\Delta J = J^+ - J' = -0.5$ (where $J^+ = N^+ - 1/2$) and $\Delta J = J^+ - J' = 1.5$ (where $J^+ = (N^+ + 1) + 1/2$) transitions are marked with an asterisk.

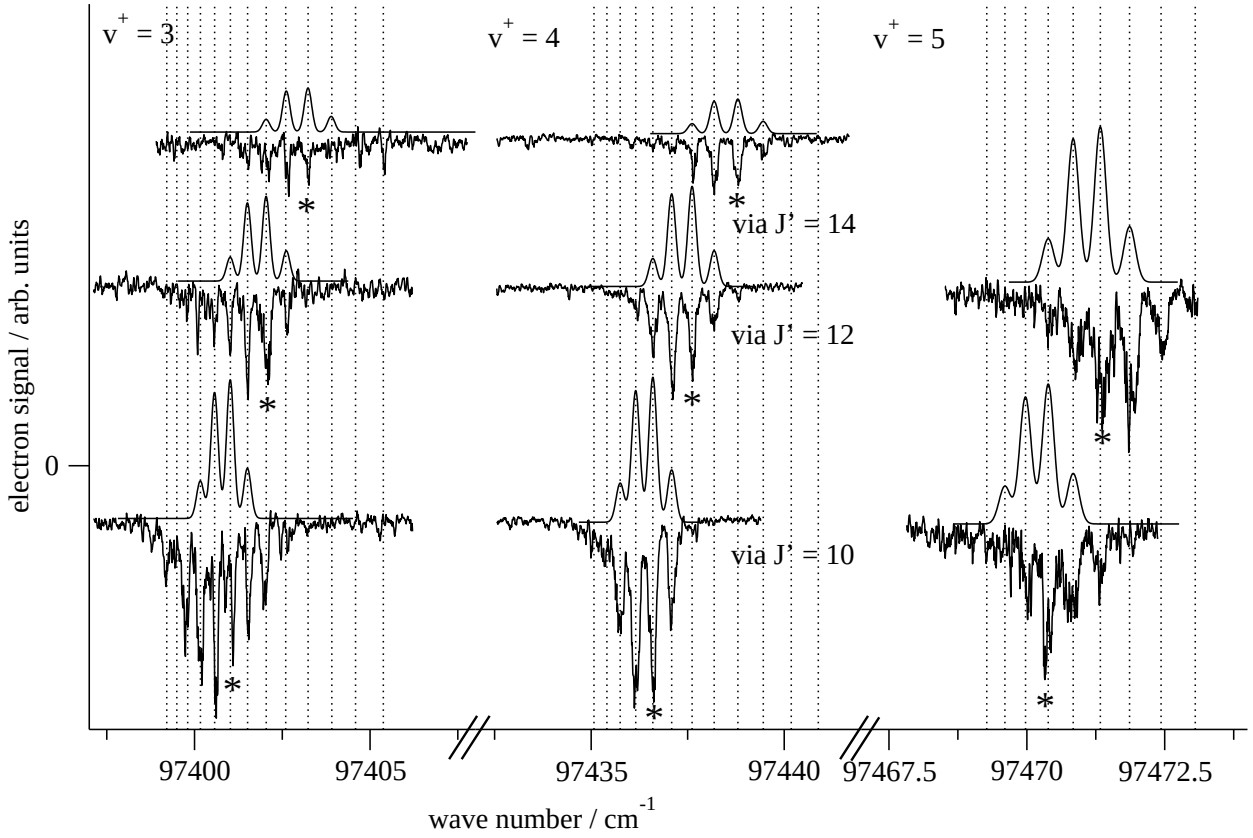

Figure 14: Rotationally resolved PFI-ZEKE photoelectron spectra of the $v^+ = 3, 4, 5$ vibrational levels of the A_1 3/2 state of $^{84}Kr^{132}Xe$ recorded via the C 0^+ ($v' = 19, J' = 10, 12, 14$) intermediate states. The experimental spectra are shown as lower, inverted traces and the calculated spectra as upper traces. The lines corresponding to the $\Delta J = J^+ - J' = 0.5$ transitions are marked with an asterisk.

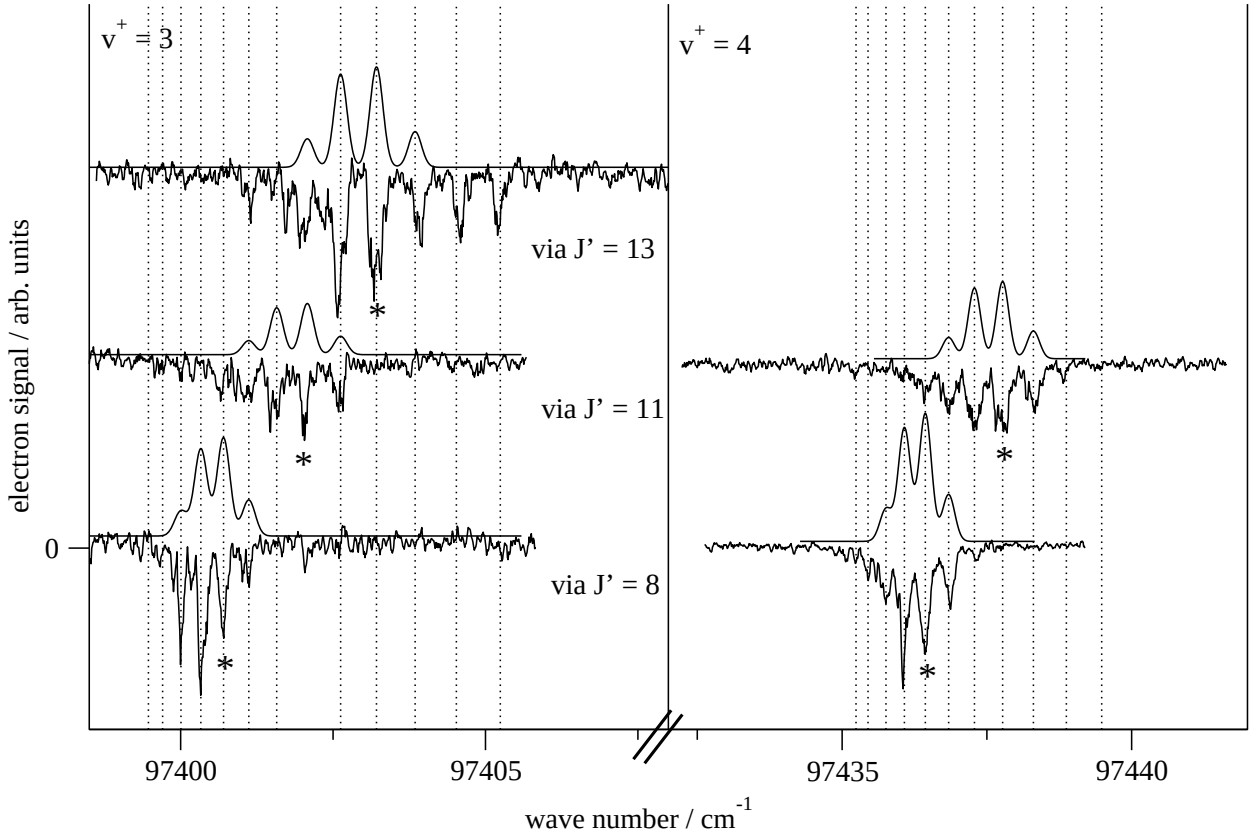

Figure 15: Rotationally resolved PFI-ZEKE photoelectron spectra of the $v^+ = 3, 4$ vibrational levels of the A_1 3/2 state of $^{84}Kr^{129}Xe$ recorded via the C 0^+ ($v' = 19, J' = 8, 11, 13$) intermediate states. The experimental spectra are shown as lower, inverted traces and the calculated spectra as upper traces. The lines corresponding to the $\Delta J = J^+ - J' = 0.5$ transitions are marked with an asterisk.

Table 1: Band origins $\tilde{\nu}_{v'0}$, rotational constants B'_v, B''_0 and centrifugal distortion constants D'_v, D''_0 derived in the analysis of the C $0^+ \leftarrow$ X 0^+ transition of $^{84}Kr^{129}Xe$, $^{84}Kr^{132}Xe$ and $^{84}Kr^{136}Xe$. All values except the normalize rms (unitless) value are in cm^{-1}.

	$^{84}Kr^{129}Xe$	$^{84}Kr^{132}Xe$	$^{84}Kr^{136}Xe$
Parameter[1]			
$\tilde{\nu}_{16,0}$	77021.830(3)	77018.991(2)	77015.340(2)
$\tilde{\nu}_{17,0}$	77058.919(2)	77056.200(1)	77052.708(1)
$\tilde{\nu}_{18,0}$	77092.307(1)	77089.726(1)	77086.410(1)
$\tilde{\nu}_{19,0}$	77122.219(2)	77119.788(2)	77116.674(1)
$\tilde{\nu}_{20,0}$	77148.829(2)	77146.572(2)	77143.669(2)
B'_{16}	0.025926(11)	0.025769(37)	0.025494(15)
$D'_{16}/10^{-7}$	0.84(9)	1.17(64)	
B'_{17}	0.025003(15)	0.024848(6)	0.024594(14)
$D'_{17}/10^{-7}$	1.01(25)	0.93(5)	
B'_{18}	0.024065(12)	0.023927(5)	0.023706(15)
$D'_{18}/10^{-7}$	1.03(18)	1.05(4)	-0.44(5)
B'_{19}	0.023079(9)	0.022973(18)	0.022745(15)
$D'_{19}/10^{-7}$		1.5(3)	
B'_{20}	0.022079(24)	0.021980(24)	0.021753(15)
$D'_{20}/10^{-7}$	1.1(5)	1.3(4)	
B''_0	0.018500318(14)	0.018335671(14)	0.0180910(144)
$D''_0/10^{-8}$	5.7456(188)	5.6491(188)	
rms value	0.37	0.35	0.44

[1]The values in parentheses represent one standard deviation in units of the last digit. The absolute uncertainty in the band centers resulting from the calibration of VUV laser wave number is estimated to be ±(0.02).

Table 2: Dissociation limits from Ref. [49] and Hund's case (c) labels of the low-lying electronic states of KrXe and $KrXe^+$. The Rydberg-state character of the electronic states of KrXe is indicated in the last column. The positions are relative to the Kr ($^1S_0$) + Xe ($^1S_0$) limit, which lies 151 cm^{-1} above the X 0^+ ($v = 0$) ground state of KrXe [50]. All values are in cm^{-1}.

dissociation limit	position	Ω	Ω	ion core + Rydberg electron
$Kr^+\ ^2P^o_{1/2}$ + Xe $^1S_0$	118 284.704	C_2 1/2		
$Kr^+\ ^2P^o_{3/2}$ + Xe $^1S_0$	112 914.434	B 1/2, C_1 3/2		
Kr $^1S_0$ + $Xe^+\ ^2P^o_{1/2}$	108 370.714	A_2 1/2		
Kr $^1S_0$ + $Xe^+\ ^2P^o_{3/2}$	97 833.790	X 1/2, A_1 3/2		
Kr $^1S_0$ + Xe $6p[1/2]_0$	80 118.962	0^+		
Kr $^1S_0$ + Xe $6p[3/2]_2$	79 212.456	2, 1, 0^+	3, 2, 1, 0^-, 0^+	$(A_1\ 3/2)\ 6p\pi$
Kr $^1S_0$ + Xe $6p[3/2]_1$	78 956.031	1, 0^-	2, 1	$(X\ 1/2)\ 6p\pi$
Kr $^1S_0$ + Xe $6p[5/2]_3$	78 403.060	3, 2, 1, 0^-	2, 1	$(A_1\ 3/2)\ 6p\sigma$
Kr $^1S_0$ + Xe $6p[5/2]_2$	78 119.798	2, 1, 0^+	1, 0^-, 0^+	$(X\ 1/2)\ 6p\sigma$
Kr $^1S_0$ + Xe $6p[1/2]_1$	77 269.144	1, 0^-		
Kr $^1S_0$ + Xe $6s'[1/2]^\circ_1$	77 185.040	1, 0^+	1, 0^-, 0^+	$(A_2\ 1/2)\ 6s\sigma$
Kr $^1S_0$ + Xe $6s'[1/2]^\circ_0$	76 196.767	0^-		
Kr $^1S_0$ + Xe $6s[3/2]^\circ_1$	68 045.156	1, 0^+	2, 1	$(A_1\ 3/2)\ 6s\sigma$
Kr $^1S_0$ + Xe $6s[3/2]^\circ_2$	67 067.547	2, 1, 0^-	1, 0^-, 0^+	$(X\ 1/2)\ 6s\sigma$
Kr $^1S_0$ + Xe $^1S_0$	0.000	X 0^+		

Table 3: Band origins $\tilde{\nu}_{v'0}$, rotational constants B'_v, B''_0, centrifugal distortion constants D'_v, D''_0, orbital hyperfine constants $h_{\Omega,v'}$ and Ω-doubling constants $q_{v'}$ for the D 1 Rydberg state of $^{84}Kr^{129}Xe$, $^{84}Kr^{132}Xe$, $^{84}Kr^{134}Xe$ and $^{84}Kr^{136}Xe$. All values except the normalize rms (unitless) value are in cm^{-1}.

Parameter[1]	$^{84}Kr^{129}Xe$	$^{84}Kr^{132}Xe$	$^{84}Kr^{134}Xe$	$^{84}Kr^{136}Xe$
$\tilde{\nu}_{m,0}$	77290.537(3)	77289.820(3)	77289.352(1)	77288.898(3)
$\tilde{\nu}_{m+1,0}$	77308.052(2)	77307.594(2)	77307.288(2)	77306.993(2)
$\tilde{\nu}_{m+2,0}$	77318.903(2)	77318.399(2)	77318.036(2)	77317.659(1)
$\tilde{\nu}_{m+3,0}$	77332.116(2)	77331.230(3)	77330.705(5)	77330.239(2)
$B'_m/10^{-2}$	2.594(3)	2.576(3)	2.564(5)	2.552(2)
$D'_m/10^{-7}$	3.1(7)	2.9(6)	2.6(3)	2.7(3)
$B'_{m+1}/10^{-2}$	2.337(2)	2.321(1)	2.318(5)	2.308(2)
$D'_{m+1}/10^{-7}$	8.2(4)	7.0(1)	7.5(2)	7.0(5)
$B'_{m+2}/10^{-2}$	2.230(3)	2.249(2)	2.281(6)	2.308(2)
$D'_{m+2}/10^{-7}$	15.5(8)	17.1(5)	21.9(12)	24.2(3)
$B'_{m+3}/10^{-2}$	2.214(7)	2.134(4)	2.093(9)	2.076(2)
$D'_{m+3}/10^{-7}$	-26.7(49)	-24.7(9)	-20.3(24)	
$h_{\Omega,m}$	-0.094(7)			
$h_{\Omega,m+1}$	-0.105(4)			
$h_{\Omega,m+2}$	-0.108(4)			
$h_{\Omega,m+3}$	-0.086(4)			
$q_m/10^{-5}$		-1.7(14)	-2.2(12)	-2.8(8)
$q_{m+1}/10^{-5}$		-2.1(8)	-2.7(11)	-2.5(8)
$q_{m+2}/10^{-5}$		3.4(9)		
$\tilde{\nu}_{*,0}$		77263.712(2)	77263.013(2)	77262.376(1)
$\tilde{\nu}_{**,0}$		77325.100(2)	77324.365(2)	77323.615(2)
$\tilde{\nu}_{***,0}$		77346.754(2)	77346.46[2]	77346.187(1)
$\tilde{\nu}_{****,0}$		77353.854(5)	77353.61[2]	
$B'_*/10^{-2}$		2.804(3)	2.800(13)	2.761(3)
$D'_*/10^{-7}$			17.9(147)	
$B'_{**}/10^{-2}$		2.460(3)	2.497(11)	2.485(3)
$D'_{**}/10^{-7}$			10.5(66)	
$B'_{***}/10^{-2}$		1.776(3)		1.749(1)
$D'_{***}/10^{-7}$		2.0(7)		1.8(3)
$B'_{****}/10^{-2}$		1.635(4)		
$q_*/10^{-5}$		-5.5(32)		
$q_{**}/10^{-5}$		-3.1(30)		
$B''_0/10^{-2}$[3]	1.8500318	1.8335671	1.8214	1.80910
$D''_0/10^{-8}$[3]	5.7456	5.6491		
rms value	0.6	0.5	0.5	0.6

[1]The values in parentheses represent one standard deviation in units of the last digit. The absolute uncertainty in the band centers resulting from the calibration of VUV laser wave number is estimated to be ±(0.02).

[2]Vibrational band intensity was insufficient for an analysis of the rotational structure and only the value of the band origin $\tilde{\nu}_{v'v''}$ could be deduced from the spectrum.

[3]Value of the ground state constant determined for the C $0^+ \leftarrow$ X 0^+ transition.

Table 4: Comparison of the experimental band origins $\tilde{\nu}_{\mathrm{exp}}$ and rotational constants B'_{exp} with the calculated band origins and rotational constants resulting from the diabatic ($\tilde{\nu}_{\mathrm{calc}}$, B_{calc}) and nonadiabatic ($\tilde{\nu}_{\mathrm{calc}^{\mathrm{na}}}$, $B_{\mathrm{calc}^{\mathrm{na}}}$) calculations of the $\Omega = 1$ states of $^{84}\mathrm{Kr}^{132}\mathrm{Xe}$. All values are in cm^{-1}.

$v' =$	*	**	m	m+1	m+2	m+3
$\tilde{\nu}_{\mathrm{exp}}$	77263.71	77325.10	77289.82	77307.59	77318.40	77331.23
$\tilde{\nu}_{\mathrm{calc}}$	77264.80	77325.76	77292.94	77307.41	77319.86	77329.69
$\tilde{\nu}_{\mathrm{calc}^{\mathrm{na}}}$	77263.43	77325.54	77292.92	77307.55	77319.16	77330.49
$B'_{\mathrm{exp}} \cdot 10^2$	2.80	2.46	2.58	2.32	2.25	2.13
$B'_{\mathrm{calc}} \cdot 10^2$	2.88	2.84	2.48	2.37	2.20	1.98
$B'_{\mathrm{calc}^{\mathrm{na}}} \cdot 10^2$	2.85	2.46	2.49	2.32	2.26	2.23

Table 5: Parameters of the diabatic $V^{\mathrm{d}}_{\mathrm{Rg},\,\mathrm{A}_2}(R)$ potential associated with the Kr(^{1}S$_0$) + Xe(6s′[1/2]$^{\mathrm{o}}_1$) dissociation limit (see text for details).

Parameter	diabatic	nonadiabatic
a[A$_2$ 1/2][1]	0.04	0.04
C_{Rep}[2] / (a.u.)	$1.95{\cdot}10^{-2}$	$1.80{\cdot}10^{-2}$
a[X 1/2][1]	0.53	0.53
$V_{ee'}$ / (cm^{-1})		13.9

[1] The potential-energy functions were taken from Ref. [9] and scaled linearly.

[2] Atomic units: 1 a.u. = $E_{\mathrm{h}}a_0^2$. The coefficient C_{Rep} had to be slightly modified upon introduction of the nonadiabatic coupling term.

Table 6: Vibronic term values $T^{v^+}_{\Lambda=0}$ and rotational constants $B^{v^+}_{\Lambda=0}$ of the X 1/2 state of $^{84}Kr^{129}Xe^+$ and $^{84}Kr^{132}Xe^+$ determined from the rotational analysis in Hund's coupling case (b).

		$^{84}Kr^{129}Xe$		$^{84}Kr^{132}Xe$	
State	v^+	$T^{v^+}_{\Lambda=0}$ [1]	$B^{v^+}_{\Lambda=0}$ [2]	$T^{v^+}_{\Lambda=0}$ [1]	$B^{v^+}_{\Lambda=0}$ [2]
X 1/2	5	-	-	95362.26(14)	0.03231(215)
	22	96782.79(9)	0.02782(52)	96776.33(9)	0.02818(52)
	28	97130.47(12)	0.02520(74)	97123.86(10)	0.02576(72)

[1] Relative uncertainties. The absolute uncertainties in the wave number calibration and the determination of the electric-field-induced shift of the ionization energies are estimated to be 0.3 cm^{-1}.

[2] Assuming $\gamma^{v^+} = -2B$.

Table 7: Vibronic term values $T_{3/2}^{v^+}$ and rotational constants $B_{3/2}^{v^+}$ of the A_1 3/2 state of $^{84}Kr^{129}Xe$ and $^{84}Kr^{132}Xe$ determined from the rotational analysis in Hund's coupling case (a).

		$^{84}Kr^{129}Xe$		$^{84}Kr^{132}Xe$	
State	v^+	$T_{3/2}^{v^+}$[1]	$B_{3/2}^{v^+}$[2]	$T_{3/2}^{v^+}$[1]	$B_{3/2}^{v^+}$[2]
A_1 3/2	3	97398.98(10)	0.02183(75)	97398.49(14)	0.02130(129)
	4	97434.76(15)	0.02120(160)	97434.08(18)	0.02117(113)
	5	-	-	97468.05(30)	0.01966(191)

[1]Relative uncertainties. The absolute uncertainties in the wave number calibration and the determination of the electric-field-induced shift of the ionization energies are estimated to be 0.3 cm^{-1}.

[2]The Λ-doubling constant is assumed to be zero for all $^2\Pi_{3/2}$ rotational levels.